INSTITUTE
FOR
AEROSPACE STUDIES

UNIVERSITY OF TORONTO

# A COMPARISON OF PILOT DESCRIBING FUNCTION MEASUREMENT TECHNIQUES



by

C. E. Frostell

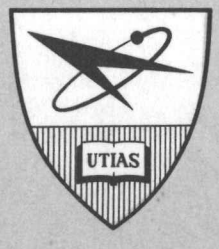


October, 1971.

UTIAS Technical Note No.167

# A COMPARISON OF PILOT DESCRIBING FUNCTION MEASUREMENT TECHNIQUES

by

C. E. Frostell

Manuscript received June, 1971.

October, 1971.

UTIAS Technical Note No. 167

ACKNOWLEDGEMENT

The author wishes to express his appreciation to his supervisor, Dr. L. D. Reid, for his support and guidance throughout the project.

The author is indebted to UTIAS for providing the opportunity to do this work. A special thanks goes to Hart House, University of Toronto and the Student Union of the Technical University in Helsinki, Finland for their student exchange program and financial support.

## SUMMARY

This work is aimed at assessing the techniques used to calculate human pilot describing functions. The study considers data analysis methods based on, (a) cross power spectral density of pilot input, output and error;

(b) cross power spectral density of pilot output and error;

(c) Fourier transform of pilot output and error.

Taped records of human pilot performance from previous investigations in a compensatory control task with random input signals of continuous power spectra were on hand and provided a pilot data base. The same data were used to exercise each method, permitting direct comparison of the results. Data are presented as amplitude and phase plots of measured describing functions using an average of a reasonably large amount of data as well as single experimental runs.

A comparison of the linear model fit parameter defined in two ways gave significant results.

TABLE OF CONTENTS

## NOTATION

| | |
|---|---|
| $A(s)$ | Transfer function of the aircraft dynamics |
| $e(t)$ | Error signal |
| $F(x(t))$ | Fourier transform of $x(t)$ |
| $i(t)$ | Input signal |
| $n(t)$ | Pilot's remnant |
| $o(t)$ | Pilot's output |
| $p(t)$ | That Pilot's output due to $n(t)$ |
| $R_{xy}(\tau)$ | The cross correlation between $x(t)$ and $y(t)$, called auto correlation if $x(t) = y(t)$ |
| $s$ | The Laplace transform variable |
| $T$ | Sampling period, sec. |
| $\bar{x}$ | The Laplace transform of $x(t)$ |
| $Y(s)$ | The pilot describing function |
| $\rho^2(\omega)$ | $1 - \dfrac{\Phi_{nn}(\omega)}{\Phi^{oo}(\omega)}$ |
| $\tau$ | Time delay, sec. |
| $\omega$ | Frequency, rad/sec. |
| $\Phi_{xy}(\omega)$ | The cross spectral density of $x(t)$ and $y(t)$ called auto power spectral density if $x(t) = y(t)$ |

## 1. INTRODUCTION

Many previous studies have investigated the human operator in a system with the task of minimizing the system error signal. The display is called compensatory if only the system error is displayed to the pilot. A block diagram of such a system is shown in Fig. 1. The difference between the input to the system and the actual state of the system is defined to be the tracking error. If the input signal has a random appearing nature and the task involves single axis tracking, then we have a single degree of freedom, random input tracking task. By changing the cut off frequency of the input power spectrum (Fig. 2), the difficulty of the task can be altered. The RMS value of the input was 0.5 in. An input with a higher cut off frequency is more difficult to track. Changing the controlled system dynamics also affects the difficulty of the task. Three different cut off frequencies and position and rate control dynamics were used in this study.

A successful approach to identifying pilot describing functions has been the frequency response measurement from a continuous servo analysis model, although sampled data models and optimal control theory models have also been used. Often pilot describing functions have been measured using the cross power spectral density of pilot input, output and error (Ref. 1 to 5). The accuracy of the result is good in most frequency ranges. However, the computer time required is considerable.

The purpose of this study is to measure the describing functions by employing the cross power spectral density of pilot output and error. This method discussed in Refs. 2, 5, 6, 7,8 and 9, is well suited for use in investigating the pilot as a single element and requires less computations than the method of cross power spectral density of input, output and error.

In Ref. 10 the use of direct Fourier transforms has been suggested and further developments are covered by Ref. 11, 12 and 13. This method has been exercised and compared to the above mentioned cross correlation methods. Use of the direct Fourier transform method allows considerable simplification in the computation. The technique, however, when applied with a random input signal is doubtful.

Other techniques for identifying the describing functions are discussed in section 7. Comparisons of some of these techniques found in the literature are summarized in section 8.

## 2. MATHEMATICAL BACKGROUND

### 2.1 Power Spectral Density Application

The basic system is shown in Fig. 1, where the human operator is a nonlinear element and the aircraft a linear element. The pilot can be represented by a linear system $Y(j\omega)$ plus a remnant term $n(t)$ as shown in Fig. 3a. Since this figure is a linear system with two inputs, $i(t)$ and $n(t)$, the superposition principle applies and the system may be represented by the sum of the systems of Fig. 3b.

One possibility is to choose the describing function $Y(j\omega)$ to minimize the RMS value of $p(t)$, the portion of the total signal being fed to the aircraft that results from the remnant. Let $Y_1(j\omega)$ correspond to minimizing of the RMS value of $p(t)$. In Refs. 1 and 2 it has been proven that in this case

$$\Phi_{in}(\omega) = 0 \text{ and } Y_1(j\omega) = \frac{\Phi_{io}(\omega)}{\Phi_{ie}(\omega)} .$$

Another possibility is to minimize the integral square value of n(t). The result is derived in Ref. 2,

$$\Phi_{en}(\omega) = 0 \text{ and } Y_2(j\omega) = \frac{\Phi_{eo}(\omega)}{\Phi_{ee}(\omega)} .$$

Since $Y_1(j\omega)$ and $Y_2(j\omega)$ are obtained by employing different criteria it is not expected that they are generally identical. In Ref. 6 the difference between these two methods is shown to be

$$Y_1(j\omega) = Y_2(j\omega) - \frac{A(-j\omega)}{1+A(-j\omega)Y_2(-j\omega)} \cdot \frac{\Phi_{n_2n_2}(\omega)}{\Phi_{ee}(\omega)}$$

where $\Phi_{n_2n_2}(\omega)$ is the auto power spectral density of the remnant n(t) related to $Y_2(j\omega)$ (minimizing of the RMS value of n(t) ).

In order to demonstrate the difference between using $Y_1(j\omega)$ and $Y_2(j\omega)$ consider the problem of identifying experimentally a system such as the human operator shown in Fig. 1. For simplicity's sake assume that in actual fact the system to be identified consists of a linear element $Y_p(j\omega)$ whose output is summed with the output of a random noise generator r(t), giving a system looking like Fig. 3a with Y replaced by $Y_p$ and n(t) by r(t). It is further assumed that i(t) and r(t) are uncorrelated.

If the identification of $Y_p(j\omega)$ is carried out through the use of $Y_1(j\omega)$ then one obtains:

$$Y_1(j\omega) = \frac{\Phi_{io}(\omega)}{\Phi_{ie}(\omega)} .$$

But $\bar{o} = \bar{e}\, Y_p(s) + \bar{r}$

$\Phi_{io}(\omega) = Y_p(j\omega)\, \Phi_{ie}(\omega)$ since $\Phi_{ir}(\omega) = 0$ and

$Y_1(j\omega) = Y_p(j\omega)$ and the identification is exact in theory.

If the identification of $Y_p(j\omega)$ is carried out through the use of $Y_2(j\omega)$ then one obtains:

$$Y_2(j\omega) = \frac{\Phi_{eo}(\omega)}{\Phi_{ee}(\omega)} .$$

But $\bar{o} = \bar{e}\, Y_p(s) + \bar{r}$

$$\Phi_{eo}(\omega) = Y_p(j\omega)\ \Phi_{ee}(\omega) + \Phi_{er}(\omega) \text{ and}$$

$$Y_2(j\omega) = Y_p(j\omega) + \frac{\Phi_{er}(\omega)}{\Phi_{ee}(\omega)} .$$

The identification is not perfect and the error involved depends on the amount of correlation between e(t) and r(t). To see the implication of this consider the following:

$$\bar{e} = \bar{i} - \bar{o}\,A(s)$$

$$\bar{o} = \bar{r} + \bar{e}\,Y_p(s)$$

$$\bar{e} = \bar{i} - \bar{r}\,A(s) - \bar{e}\,AY_p(s) \text{ or } \bar{e} = \frac{\bar{i}}{1+AY_p(s)} - \frac{\bar{r}\,A(s)}{1+AY_p(s)}$$

$$\Phi_{ee}(\omega) = \frac{1}{|1+AY_p(j\omega)|^2}\,\Phi_{ii}(\omega) + \frac{|A(j\omega)|^2}{|1+AY_p(j\omega)|^2}\,\Phi_{rr}(\omega)$$

(since $\Phi_{ir}(\omega) = 0$)

$$\text{and } \Phi_{er}(\omega) = \frac{-A^*(j\omega)}{(1+AY_p(j\omega))^*}\,\Phi_{rr}(\omega)$$

$$Y_2(j\omega) = Y_p(j\omega) - \frac{A^*(j\omega)\Phi_{rr}(\omega)|1 + AY_p(j\omega)|^2}{(1+AY_p(j\omega))^*\,\{\Phi_{ii}(\omega)+|A(j\omega)|^2\Phi_{rr}(\omega)\}}$$

if $\Phi_{ii}(\omega) \gg \Phi_{rr}(\omega)$ then $Y_2(j\omega) = Y_p(j\omega)$ and

if $\Phi_{ii}(\omega) \ll \Phi_{rr}(\omega)$ then $Y_2(j\omega) = -\frac{1}{A(j\omega)}$. Thus the extent of the measurement error depends on the size of $\Phi_{rr}(\omega)$ relative to $\Phi_{ii}(\omega)$.

The model used in this example is often put forward as a reasonable approximation to the human operator. This indicates that care must be taken if $Y_2(j\omega)$ is used to find human operator describing functions. In the event that another form of nonlinear system is under study, it is not possible to indicate from the above analysis whether $Y_1(j\omega)$ or $Y_2(j\omega)$ is more useful.

## 2.2 Direct Fourier Transforms

In Ref. 10 it is suggested that a direct Fourier transform can be used to measure pilot describing functions. The cross power spectral density method is employed by Fourier transforming the cross correlation between two signals x(t) and y(t) that are non-zero between $\pm$ T.

$$\text{Estimate of } R_{xy}(\tau) = \frac{1}{2T}\int_{-T}^{T} x(t)y\,(t+\tau)dt$$

$$\text{Estimate of } F(x(t)\,) = \int_{-T}^{T} e^{-j\omega t}\,x(t)dt$$

$$\text{Estimate of } \Phi_{xy_1}(\omega) = \int_{-2T}^{2T} \left\{ \frac{1}{2T}\int_{-T}^{T} x(t)y(t+\tau)dt \right\} e^{-j\omega\tau}\,d\tau$$

Note that the $\pm$ 2T limits come from the fact that $-2T < \tau < 2T$. However, this estimate of the cross power spectral density of x(t) and y(t) is a very bad estimate, not usually used when the cross correlation technique is employed with random signals. In section 4 the estimate of $\Phi_{xy}(\omega)$ used in this experiment and in Refs. 1, 2 and 3 is outlined.

In Refs. 10, 12 and 13 it is shown that

$$\Phi_{xy_2}(\omega) = \frac{F^*[x]\ F[y]}{2T} =$$

$$\left\{\int_{-T}^{T} x(t)e^{-j\omega t}\,dt\right\}\left\{\int_{-T}^{T} y(\tau)e^{-j\omega\tau}\,d\tau\right\}\ \frac{1}{2T}$$

is identical to $\Phi_{xy_1}(\omega)$. Following this the describing functions are identified from

$$Y_3(j\omega) = \frac{\Phi_{io_2}(\omega)}{\Phi_{ie_2}(\omega)} = \frac{1/2T\ F^*[i]\ F[o]}{1/2TF^*[i]\ F[e]} = \frac{F[o]}{F[e]}\ .$$

It will be shown in section 6.1 that this estimate of power spectrum leads to large variability in the data when applied to random signals. If the proof in Refs. 10, 12 and 13, showing that $\Phi_{xy_1}(\omega)$ is identical to $\Phi_{xy_2}(\omega)$, is assumed to hold in the case of the exact formulation for power spectral density, then it is, as shown in Appendix A, possible to prove that any two signals are correlated unless one of them is identically zero, thus indicating that the original function chosen ($\Phi_{xy_1}$) was a bad estimate of power spectral density.

According to Refs. 10 to 13 the linear fit parameter

$$\rho^2(\omega) = \frac{|\Phi_{io_2}(\omega)|^2}{\Phi_{ii_2}(\omega)\ \Phi_{oo_2}(\omega)} = \frac{F^*[i]\ F[o]\ F[i]\ F^*[o]}{F^*[i]\ F[i]\ F^*[o]\ F[o]} = 1.0$$

This erroneously indicates linearity under all circumstances.

However it is felt that direct Fourier transforms are a valid interpretation under the following conditions (Ref. 14):

1. The input is a sum of sine waves

2. The transforms are evaluated using the same sine and cosine functions for both transforms over the same run length

3. The transforms are evaluated only at the input frequencies.

Beyond these restrictions the use of the direct transforms is questionable.

## 3. LINEAR FIT PARAMETERS

Since the controlled vehicle is a linear system, with the transfer function $A(j\omega)$, we define a linear fit parameter $\rho(\omega)$ to measure the linearity of the human operator alone. If the pilot behaves in a nearly linear fashion, then $\rho(\omega)$ will have values close to unity and the remnant will be small, while low values of $\rho(\omega)$ indicate more nonlinear performance and the corresponding remnant will be large.

### 3.1 $\rho_1^2$ when $Y_1(j\omega)$ Is Used

In Fig. 3a $n_1(t)$ is the remnant and is uncorrelated with the input $i(t)$.

Define
$$\rho_1^2(\omega) = 1 - \frac{\Phi_{n_1 n_1}(\omega)}{\Phi_{oo}(\omega)}$$

where $\Phi_{n_1 n_1}(\omega)$ is the auto power spectral density of the remnant related to the minimizing of the RMS value of $p(t)$. From Fig. 3a $\bar{n}_1 = \bar{o} - \bar{e}\, Y_1(s)$

$$\Phi_{n_1 n_1}(\omega) = \Phi_{oo}(\omega) + |Y_1(j\omega)|^2 \Phi_{ee}(\omega) - Y_1(j\omega)^* \Phi_{eo}(\omega) - Y_1(j\omega)\, \Phi_{oe}(\omega)$$

Since $\Phi_{eo}(\omega) = \Phi_{oe}(\omega)^*$

$$\Phi_{n_1 n_1}(\omega) = \Phi_{oo}(\omega) + |Y_1(j\omega)|^2 \Phi_{ee}(\omega) - Y_1(j\omega)^*\, \Phi_{oe}(\omega)^* - Y_1(j\omega)\, \Phi_{oe}(\omega)$$

$$= \Phi_{oo}(\omega) + |Y_1(j\omega)|^2 \Phi_{ee}(\omega) - 2\,\mathrm{Re}\left\{ Y_1(j\omega)\, \Phi_{oe}(\omega) \right\}$$

$$= \Phi_{oo}(\omega) + |Y_1(j\omega)|^2 \Phi_{ee}(\omega) - 2\left[ \mathrm{Re}[Y_1]\,\mathrm{Re}\left\{ \Phi_{oe}(\omega) \right\} - \mathrm{Im}\{Y_1\}\,\mathrm{Im}\left\{ \Phi_{oe}(\omega) \right\} \right]$$

$$\rho_1^2(\omega) = 1 - \frac{\Phi_{n_1 n_1}(\omega)}{\Phi_{oo}(\omega)} = -|Y_1(j\omega)|^2 \frac{\Phi_{ee}(\omega)}{\Phi_{oo}(\omega)} + 2\,\frac{1}{\Phi_{oo}(\omega)} \left[ \mathrm{Re}\{Y_1\}\,\mathrm{Re}\left\{ \Phi_{oe}(\omega) \right\} - \mathrm{Im}\{Y_1\}\,\mathrm{Im}\left\{ \Phi_{oe}(\omega) \right\} \right]$$

From Fig. 3a $\bar{o} = Y_1(s)\,(\bar{i} - A(s)\,\bar{o}) + \bar{n}_1$

$$\bar{o} = \frac{Y_1(s)\,\bar{i} + \bar{n}_1}{1 + A(s)Y_1(s)}$$

When $i(t)$ and $n_1(t)$ are assumed uncorrelated then $\Phi_{in_1}(\omega) = 0$

$$\Phi_{oo}(\omega) = \left| \frac{Y_1(j\omega)}{1+AY_1(j\omega)} \right|^2 \Phi_{ii}(\omega) + \left| \frac{1}{1+AY_1(j\omega)} \right|^2 \Phi_{n_1 n_1}(\omega)$$

$$\rho_1^2(\omega) = 1 - \frac{\Phi_{n_1n_1}(\omega)}{\Phi_{oo}(\omega)} = \frac{\left|\frac{Y_1(j\omega)}{1+AY_1(j\omega)}\right|^2 \Phi_{ii}(\omega) + \left(\left|\frac{1}{1+AY_1(j\omega)}\right|^2 - 1\right)\Phi_{n_1n_1}(\omega)}{\left|\frac{Y_1(j\omega)}{1+AY_1(j\omega)}\right|^2 \Phi_{ii}(\omega) + \left|\frac{1}{1+AY_1(j\omega)}\right|^2 \Phi_{n_1n_1}(\omega)}$$

If $\Phi_{n_1n_1}(\omega) \ll \Phi_{ii}(\omega)$ then $\rho_1^2 \to 1.0$ and the linear model is a perfect fit.

If $\Phi_{n_1n_1}(\omega) \gg \Phi_{ii}(\omega)$ then $\rho_1^2 \to 1 - /1 + AY_1(j\omega)/^2$ and does not go to zero as one might anticipate.

3.2 $\rho_2^2$ when $Y_2(j\omega)$ Is Used

From Fig. 3a we obtain, $\bar{o} = \bar{n}_2 + Y_2(s)\,\bar{e}$

$\Phi_{oo}(\omega) = \Phi_{n_2n_2}(\omega) + /Y_2(j\omega)/^2 \Phi_{ee}(\omega)$ since it was found when $Y_2(j\omega) = \frac{\Phi_{eo}(\omega)}{\Phi_{ee}(\omega)}$ (minimizing the RMS value of n(t) ) (Ref. 2) that $n_2(t)$ has zero correlation with e(t), i.e., $\Phi_{en_2}(\omega) = 0$.

Again define $\rho_2^2(\omega) = 1 - \frac{\Phi_{n_2n_2}(\omega)}{\Phi_{oo}(\omega)} = |Y_2(j\omega)|^2 \frac{\Phi_{ee}(\omega)}{\Phi_{oo}(\omega)}$

$$\rho_2^2(\omega) = \frac{|\Phi_{eo}(\omega)|^2}{\Phi_{ee}(\omega)\Phi_{oo}(\omega)}$$

Now since $\Phi_{en_2}(\omega) = 0$ then $\Phi_{oo}(\omega) = \Phi_{n_2n_2}(\omega) + /Y_2(j\omega)/^2 \Phi_{ee}(\omega)$

$$\rho_2^2(\omega) = /Y_2(j\omega)/^2 \cdot \frac{\Phi_{ee}(\omega)}{\Phi_{oo}(\omega)} = \frac{|Y_2(j\omega)|^2 \Phi_{ee}(\omega)}{\Phi_{n_2n_2}(\omega) + |Y_2(j\omega)|^2 \Phi_{ee}(\omega)}$$

If $\Phi_{n_2n_2}(\omega) \ll \Phi_{ee}(\omega)$ then $\rho_2^2 \to 1.0$

If $\Phi_{n_2n_2}(\omega) \gg \Phi_{ee}(\omega)$ then $\rho_2^2 \to 0$ and thus behaves as expected.

3.3 A Comparison of $\rho^2$ Defined in Two Ways

From Fig. 3b we obtain $\bar{p} = \bar{n} - \bar{p}\,A(s)\,Y(s)$, $\bar{n} = (1 + A(s)Y(s))\bar{p}$

$\Phi_{nn}(\omega) = |1 + AY(j\omega)|^2 \Phi_{pp}(\omega)$. If in practice

$$Y_1 = \frac{\Phi_{io}(\omega)}{\Phi_{ie}(\omega)}$$

is quite close to

$$Y_2 = \frac{\Phi_{eo}(\omega)}{\Phi_{ee}(\omega)}$$

then $Y_1 = Y_2 = Y$, $n_1 = n_2 = n$ and $p_1 = p_2 = p$. (This will be shown true for the present data in section 6).

Define $\rho^2(\omega) = 1 - \frac{\Phi_{pp}(\omega)}{\Phi_{oo}(\omega)}$. Then in the case where $Y_1 = Y_2 = Y$

$$\rho^2(\omega) - \rho_1^2(\omega) = \rho^2(\omega) - \rho_2^2(\omega) = \frac{\Phi_{nn}(\omega) - \Phi_{pp}(\omega)}{\Phi_{oo}(\omega)} = \left[ |1+AY(j\omega)|^2 - 1 \right] \frac{\Phi_{pp}(\omega)}{\Phi_{oo}(\omega)} =$$

$$\doteq \left[ |1+AY(j\omega)|^2 - 1 \right] (1-\rho^2(\omega))$$

also $\rho^2(\omega) = \frac{|\Phi_{io}(\omega)|^2}{\Phi_{ii}(\omega)\Phi_{oo}(\omega)}$ (Ref. 1)

In the past $\rho^2$ has usually been used when employing $Y_1(j\omega) = \frac{\Phi_{io}(\omega)}{\Phi_{ie}(\omega)}$.

In this case it can be shown by using the equations of section 3.1 that

$$\rho^2(\omega) = \frac{|Y_1(j\omega)|^2 \Phi_{ii}(\omega)}{|Y_1(j\omega)|^2 \Phi_{ii}(\omega) + \Phi_{n_1 n_1}(\omega)}$$

If $\Phi_{n_1 n_1}(\omega) \ll \Phi_{ii}(\omega)$ then $\rho^2 \rightarrow 1.0$

If $\Phi_{n_1 n_1}(\omega) \gg \Phi_{ii}(\omega)$ then $\rho^2 \rightarrow 0$ and thus behaves as expected.

Now $\rho_1^2$ or $\rho_2^2$ can be found from $\rho^2(\omega) - \left\{ |1+AY(j\omega)|^2 - 1 \right\} \left\{ 1-\rho^2(\omega) \right\} = \rho_3^2(\omega)$

Figure 4 is a sample comparison of single run $\rho_1^2$, $\rho_2^2$ and $\rho_3^2$ (based on $\rho_1^2$ as defined in section 3.1, and

$$\rho_2^2 = \frac{|\Phi_{eo}(\omega)|^2}{\Phi_{ee}(\omega)\Phi_{oo}(\omega)} \quad ).$$

The fit is good except for the first few frequency points. In Ref. 1 it was shown that the experimental accuracy in calculating $\rho^2$ for the low frequency points is poor. In this experiment $\rho_3^2$ is calculated with $\rho^2$ as a base

( $\rho_3^2(\omega) = \rho^2(\omega) + (|1+AY(j\omega)|^2 - 1)(1-\rho^2(\omega))$ ).

Since for the low frequency points, especially in a rate control task, the term $|1 + AY(j\omega)|^2 - 1$ is large and is multiplied by a very small number $(1-\rho^2)$, a small error in $\rho^2$ causes a very large error in $\rho_3^2$. In this study $\rho_3^2$ has been used as

a measure of the linear model fit when

$$Y_1 = \frac{\Phi_{io}(\omega)}{\Phi_{ie}(\omega)} \quad \text{is employed.}$$

As shown in Fig. 4 the equivalent $\rho_1^2$ is more accurate at the first few low frequency points than $\rho_3^2$. Therefore it is suggested that $\rho_1^2$ should be used in future studies based on

$$Y_1(j\omega) = \frac{\Phi_{io}(\omega)}{\Phi_{ie}(\omega)}$$

if $\Phi_{n_1 n_1}(\omega) \ll \Phi_{ii}(\omega)$.

The model fit parameters $\rho_1^2$ and $\rho_2^2$ are based on the remnant n(t). A small remnant will give $\rho_1^2$ and $\rho_2^2$ close to unity, thus indicating close to linear behaviour. In a physical sense this is an excellent measure of the linearity of the pilot alone. In Figs. 15 and 19 $\rho_2^2$ is shown.

If we are interested in the system from a control system engineering point of view then we are more interested in the signal going into the aircraft and especially the portion p(t) due to the remnant. $\rho^2$ (based on p(t) ) is a good measure of linearity in this case.

## 4. EXPERIMENTAL SET UP

Data from earlier experiments at UTIAS (Ref. 1) were used. The equipment used to provide this data has been described in detail in Ref. 1. The main parameters will be repeated here.

The facility used consisted of a modified CF-100 fixed-base flight simulator cockpit coupled with an EAI TR-48 analogue computer. The signals i(t), o(t) and e(t) were recorded in digital form after passing through an EECO ZA37050 analogue-to-digital converter. The sampling rate was 20 samples per second. Of the 190 seconds long experimental run, 180 seconds (T) were recorded and used. The maximum length of lag in terms of samples (NLAGS) was 200 giving $\tau_m = 9.95$ seconds in the correlation functions. The general procedure was to find the auto or cross correlation $R_{xy}(\tau)$, then multiplying this by a particular function $\alpha(\tau)$ before estimating $\Phi_{xy}(\omega)$ by Fourier transforming $R_{xy}(\tau)$. This leads to more acceptable spectral window shapes. Here the "Hanning window" was used ($\alpha(\tau) = \frac{1}{2}(1 + \cos(\pi\tau/\tau_m))$). (For further details see Ref. 1).

Only compensatory data were analyzed here. The aircraft dynamics were a) position control (0.114 in/deg) and b) rate control (0.338/s in/deg/sec as measured from joystick input by the pilot to display motion). Both cases (K and $1/s$) were further divided into three parts depending upon the cut off frequency of the random input signal. Low (2 rad/sec), medium (4 rad/sec) and high (6 rad/sec) cut off frequencies were used. Figure 2 shows the spectral shape of these input signals (L, M and H).

Initially each of these six conditions consisted of six experimental runs by each of six subjects, i.e., 36 runs per condition. A few runs had to be skipped due to bad recording. Table 1 shows the number of runs to calculate

the means and standard deviations for each condition.

The spectral calculations were done on an IBM 7094 computer. The describing function $Y_1(j\omega)$ and corresponding $\rho^2(\omega)$ for one run required 57.9 seconds. Some simplifications could be done to calculate $Y_2(j\omega)$ and $\rho_2^2(\omega)$. The time used to analyze one run was 39.5 seconds allowing a time saving of 32%. In this experiment a normal Fourier transform was used to calculate $Y_3(j\omega)$. At the end of the experiment a trial with a fast Fourier transform was performed requiring only 5.9 seconds to analyze one run. The time saving was 90% over the $Y_1(j\omega)$ calculation. Note that no $\rho^2$ calculation is performed in the case of $Y_3(j\omega)$. All calculations used the same time records and found the pilot describing function at 25 frequency points.

## 5. IDENTIFICATION OF AN ANALOG PILOT

An analog pilot, $Y(s) = 87.5/(s + 3)$ deg/in, performed experimental runs utilizing the normal experimental set up and input signal levels. The result, Fig. 5, gives us an insight into the accuracy with which the digital programs (Fourier transforms and cross power spectral density of output and error) can identify pilot describing functions. The top of the triangal symbol locates the data positions. As in Ref. 1 where the cross power spectral density of input, output and error was used, no problems were encountered with the position control task. In the rate control tasks the performance was excellent except for the first frequency point. This problem is due to low power levels for the signals $o(t)$ and $e(t)$ as described in Ref. 1.

## 6. RESULTS

Figures 6 to 11 show the amplitude and phase plots of the describing function $Y_3(j\omega)$, i.e., data analyzed by Fourier transforms of the output signal and error signal as described in section 2.2. In the figures K stands for position control and 1/s for rate control. In the amplitude plots the left corner and in the phase plots the right corner of the triangle symbol indicates the mean and the bars show plus and minus one standard deviation. Figures 12 to 14 and 16 to 18 show the amplitude and phase plots of the describing function when the analyzing process is based on cross power spectral density of output and error. The model fit parameter $\rho_2^2$ (calculated from $|\Phi_{eo}(\omega)|^2/\Phi_{ee}(\omega)\Phi_{oo}(\omega)$ ) plus and minus one standard deviation is shown in Figs. 15 and 19, where the right corner of the triangle symbol indicates the mean. The describing function $Y_1(j\omega)$, based on cross power spectral density of input, output and error has been plotted ($\pm$ one $\delta$) in Ref. 1 for the same experimental data (see Figs. 36 and 37).

### 6.1 Comparison of Variation

As shown in Figs. 12 to 14 and 16 to 18 the variation in the describing function when cross power spectral density of output and error is employed, is small and smooth and very close to the result in Ref. 1 (Figs. 36 and 37), where cross power spectral density of input, output and error was used. When Fourier transforms are used, Figs. 6 to 11, the variation is large and rough.

The cross power spectral density methods use data from a short experimental run and attempt to predict the pilot describing function that would be found for an infinitely long run. The variation from one experimental run to

another is expected to be small and smooth. On the other hand if $Y_3(j\omega)$ and e(t) is given for a particular run, then o(t) can be calculated exactly from $Y_3(j\omega)$ = F(o)/F(e) for that particular 3 min. run, since the Fourier transform technique calculates the describing function that fits the short experimental interval exactly and thus the variation from run to run is large (when random inputs are used), although the means of a large number of experimental runs can be expected to approach the desired describing function.

## 6.2 Comparison of Means

The means of $Y_1(j\omega)$, $Y_2(j\omega)$, $Y_3(j\omega)$ and corresponding model fit parameters are plotted in Figs. 20 to 27. The cross spectral density methods ($Y_1(j\omega)$ and $Y_2(j\omega)$ ) are very close to each other over the whole frequency range for all six conditions. $Y_1(j\omega)$ and the corresponding $\rho_1^2$ (calculated as $\rho_3^2$) are plotted as a line. $Y_2(j\omega)$ and the corresponding $\rho_2^2$ are represented by a triangle symbol, where the top is the data position. $Y_3(j\omega)$ is plotted as a plus sign. The means of $\rho^2$ as measured in Ref. 1 are represented by a cross.

The Fourier transforms technique ($Y_3(j\omega)$ ) gives a good approximation of the pilot describing function if a large number of runs are averaged although the large variance in the data reduces its usefulness.

The above mentioned results are verified in Figs. 28 to 35, where the pilot describing functions based on one experimental run per condition by the same typical subject, have been plotted.

The linear fit parameters $\rho_1^2$ and $\rho_2^2$ show a pilot behaviour quite close to linear. The plots are quite flat and close to unity. This indicates a fairly constant remnant n(t). Since $\rho^2$ in Ref. 1 drops off in the middle of the frequency range, p(t) is built up in the closed loop system.

# 7. OTHER METHODS FOR MEASURING PILOT DESCRIBING FUNCTIONS

Techniques for identifying describing functions other than those used in this experiment will briefly be described in this section. In section 8 comparisons found in the literature are discussed.

## 7.1 Parameter Model

The parameter model method assumes a particular describing function model for the pilot dynamics and then solves for the parameters in that model. With proper programming the parameters can be made to converge to values which minimize the difference between system and model outputs. Although the stability and speed of convergence of such parameter trackers is of concern, the technique has the advantages of being physically easy and inexpensive to implement (requiring only an analog computer). The method is restricted in that only a limited set of systems, which have the specified form, can be adequately identified.

The model used in Ref. 15 has the form

$$Y(s) = \frac{a_3 s + a_4}{s^2 + a_1 s + a_2} \cdot e^{-\lambda s}$$

where the time shift $\lambda$ accounts for any pure time delay in Y(s). Estimates of the parameters $a_1$, $a_2$, $a_3$, and $a_4$ were determined by a quasilinearization technique described in Ref. 15.

In Ref. 16 two different model forms were used. The three parameter model was

$$Y(s) = \frac{\frac{K_1}{\tau}\left(1 + \frac{K_2}{\tau}s\right)}{\left(1 + \frac{1}{\tau}s\right)^2}$$

and the two parameter model was $Y(s)\,A(s) = \frac{K\,e^{-\tau s}}{s}$. This model is called the crossover model as developed in Ref. 17.

## 7.2 Orthogonal Filters

The orthogonal filter method (Ref. 18) is somewhat more general than the parameter model. It assumes that the unknown system dynamics can be modelled by a series of transfer functions of the form (Ref. 15)

$$Y(s) = e^{-\lambda s}\left\{\frac{b_1}{\tau_1 s + 1} + \frac{b_2(\tau_1 s-1)}{(\tau_1 s+1)(\tau_2 s+1)} + \frac{b_3(\tau_1 s-1)(\tau_2 s-1)}{(\tau_1 s+1)(\tau_2 s+1)(\tau_3 s+1)} + \cdots\right\}$$

Estimates of the parameters $b_1, b_2, b_3, \ldots$ etc., can be determined by a multiregression technique (Ref. 7).

## 7.3 Impulse Response

The impulse response method (Refs. 7, 9, 12 and 19) assumes a very general input-output relationship that can be represented by the form (Ref. 15)

$$Y(s) = e^{-\lambda s}\int_0^{\tau_m} g(\tau)e^{-\tau s}\,d\tau$$

where $g(\tau)$ is an impulse response function that is assumed to be zero for $\tau < 0$ and also zero for $\tau > \tau_m$. The calculation of the impulse response function at discrete times, $g(o)$, $g(\Delta t)$, $g(2\Delta t)$, etc., is shown in Ref. 15.

# 8. COMPARATIVE EXPERIMENTS IN THE LITERATURE

A few comparisons of techniques for measuring pilot describing functions can be found in the literature. The techniques of Fourier transforms, parameter models, orthogonal filters and cross power spectral density are covered in Ref. 16. However, the experiment compared techniques on single runs only and thus there is no variation in the data shown. Furthermore the input was in all cases of sum of sinusoids. These methods provided good measurements in the region of system crossover frequency. This is the frequency where the product of the absolute values of the pilot dynamics and of the aircraft dynamics passes from greater than unity to less than unity. The more computationally expensive techniques provided more accurate results away from crossover. All methods

deteriorated when signal levels were low. Controlled dynamics of the form $1/s$ or $1/s^2$ and the pilot's ability to control either very well or poorly reduced signal levels over certain frequency ranges outside the region of crossover frequency.

In Fig. 38 (from Ref.16) the Fourier transform method is compared to the two and three parameters model for an analog pilot (known system). The Fourier transform technique is good (since the input is a sum of sinusoids) but the parameter models are accurate only in the region of crossover.

In Fig. 39 (from Ref. 16) the Fourier transform, two and three parameters models, orthogonal filters and cross correlation are compared for a human pilot. Since this comparison is based on a single run and no variation in the describing function based on different techniques can be shown, it is difficult to draw any conclusions.

In Ref. 15 three different identification methods (the parameter model, orthogonal filters, and impulse-response techniques) were applied to the identification of both simulated (i.e., known) systems and piloted systems. According to Ref. 15 the three methods were shown to estimate adequately the pilot describing functions. However, the input signals were a sum of sinusoids. No variation of the describing functions could be shown since the experiment consisted of a single run per condition.

In Ref. 17 the two parameter model (the crossover model) is compared to the cross spectral density of input, output and error. Figure 40 shows a typical pilot comparison from Ref. 17. The fit is good as long as the input power in the region of crossover is high enough to allow accurate parameter tracking. In Fig. 40 the input signal had a power spectrum with a cut off frequency of 4 rad/sec (M). A cut off frequency of 2 rad/sec (L) was also used in this experiment. No comparison of variations of the describing functions was done.

## 9. CONCLUSIONS

1. The overall agreement between the pilot describing function measured by cross power spectral density of input, output and error and by cross power spectral density of output and error is very good. This second technique can successfully be used to measure the pilot describing function and the linear model fit parameter, when the nonlinear and noise components are small. This technique allows a 32% saving in computer time.

2. If a large amount of data is available, the Fourier transforms method gives a good approximation to the mean, although the large variance reduces its usefulness as an experimental technique (when random inputs are employed) relative to other approaches. The computer time saving was 90% as compared to the cross spectral density method of input, output and error.

3. As a measure of the linearity of the human pilot, the linear model fit parameters $\rho_1^2(\omega)$ and $\rho_2^2(\omega)$ based on the remnant $n(t)$, are preferable to $\rho^2$, provided that $\Phi_{ii}(\omega) \gg \Phi_{n_1 n_1}(\omega)$ and $\Phi_{ee}(\omega) \gg \Phi_{n_2 n_2}(\omega)$.

## REFERENCES


1. Reid, L. D. — "The Measurement of Human Pilot Dynamics in a Pursuit Plus Disturbance Tracking Task". UTIAS Rept. No.138, University of Toronto, April 1969.

2. Reid, L. D. — "The Design of a Facility for the Measurement of Human Pilot Dynamics". UTIAS Tech.Note No.95, University of Toronto, June 1965.

3. Gordon-Smith, M. — "An Investigation into Certain Aspects of the Describing Function of a Human Operator Controlling a System of One Degree of Freedom". UTIAS Rept. No. 149, University of Toronto, Feb, 1970.

4. McRuer, D. T.<br>Krendel, E. S. — "Dynamic Response of Human Operators". WADC TR 56-524, October 1957.

5. McRuer, D. T.<br>Graham, D.<br>Krendel, E. S.<br>Reisener, W. Jr., — "Human Pilot Dynamics in Compensatory Systems". AFFDL-TR-65-15, July 1965.

6. Elkind, J. I. — "A Comparison Between Open and Closed-Loop Measurements of Dynamics Systems". Bolt, Beranek and Newman Inc. Memorandum Rept. 8224-4, March 1963.

7. Elkind, J. I. — "Further Studies of Multiple Regression Analysis of Human Pilot Dynamic Response. A Comparison of Analysis Techniques and Evaluation of Time-Varying Measurements". ASD-TDR-63-618, March 1964.

8. Wingrove, R. C.<br>Edwards, F. G. — "Measurement of Pilot Describing Functions From Flight Test Data with an Example from Gemini X". Fourth Annual NASA-University Conference on Manual Control. NASA SP-192, March 1968, pp.119-134.

9. Wingrove, R. C.<br>Edwards, F. G. — "A Technique for Identifying Pilot Describing Functions from Closed-Loop Operating Records". NASA TN D-6235, March 1971.

10. Taylor, L. W. Jr., — "Discussion of Spectral Human-Response Analysis". Second Annual NASA - University Conference on Manual Control. NASA SP-128, March 1966, pp.403-412.

11. Smith, H. J. — "Human Describing Functions Measured in Flight and on Simulators". Second Annual NASA - University Conference on Manual Control. NASA SP-128, March 1966, pp.279-290.

12. Taylor, L. W. Jr., — "A Comparison of Human Response Modelling in the Time and Frequency Domains". Third Annual NASA - University Conference on Manual Control. NASA SP-144, March 1967, pp.137-153.

13. Taylor, L. W. Jr., "Relationships Between Fourier and Spectral Analysis". Third Annual NASA - University Conference on Manual Control. NASA SP-144, March 1967, pp.183-186.

14. Young, L. R.
Windblade, R. "Summary". Second Annual NASA - University Conference on Manual Control. NASA SP-128, March 1966, pp. 1-11.

15. Wingrove, R. C. "Comparison of Methods for Identifying Pilot Describing Functions from Closed-Loop Operating Records". NASA TN D-6235, March 1971.

16. Shirley, R. S. "A Comparison of Techniques for Measuring Human Operator Frequency Response". Sixth Annual NASA - University Conference on Manual Control. AFIT, AFFDL, 1970, pp.803-869.

17. Jackson, G. A. "Measuring Human Performance with a Parameter Tracking Version of the Crossover Model". NASA CR-910, October 1967.

18. Elkind, J. I.
Starr, E. A.
Green, D. M.
Darley, D. L. "Evaluation of a Technique for Determining Time-Invariant and Time-Variant Dynamic Characteristics of Human Pilots". NASA TN D-1897, May 1963.

19. Goodman, T. P. "Determination of System Characteristics from Normal Operating Records". Transaction ASME, February 1956.

## APPENDIX A

Consider two independent stationary random signals x(t) and y(t) with amplitude probability functions that are symmetric about zero.

$P_1(x)$ is symmetric about $x = 0$

$P_2(y)$ is symmetric about $y = 0$

$$\int_{-\infty}^{\infty} P_1(x)\, x\, dx = 0$$

and

$$\int_{-\infty}^{\infty} P_2(y)\, y\, dy = 0$$

Now

$$R_{xy}(\tau) = \lim_{T\to\infty} \frac{1}{2T}\int_{-T}^{T} x(t)\, y(t+\tau)\, dt$$

$$= \int_{-\infty}^{\infty}\int_{-\infty}^{\infty} P_1(x)P_2(y)\, xy\, dxdy \quad \left\{ \begin{array}{l} \text{since } P(x/y) = P_1(x) \\ \text{because x(t) and y(t)} \\ \text{are assumed independent.} \end{array} \right\}$$

$$= 0$$

And

$$\Phi_{xy}(\omega) = \frac{1}{2\pi}\int_{-\infty}^{\infty} R_{xy}(\tau)\, e^{-j\omega\tau}\, d\tau$$

$$= 0 \qquad R_{xy}(\tau) \equiv 0$$

However this does not require $\Phi_{xx}(\omega)$ or $\Phi_{yy}(\omega) = 0$

Now consider the identical situation but apply the assumption that

$$\Phi_{xy}(\omega) = \lim_{T\to\infty} \frac{1}{2T}\, F^*(x)\, F(y)$$

for $\Phi_{xy}(\omega) = 0$ for all $\omega$

requires $\lim_{T\to\infty} \frac{1}{2T}\, F^*_\tau(x)\, F_\tau(y) = 0$

or that either $F^*_\tau(x)$ or $F_\tau(y) = AT^\epsilon$

where A is a constant and $\epsilon < 1/2$ as $T\to\infty$

which means that either

$$\Phi_{xx}(\omega) \text{ or } \Phi_{yy}(\omega) = 0 \text{ for all } \omega .$$

According to this it is impossible to have two completely uncorrelated signals unless one of them is identically zero. As shown above this is not true.

TABLE 1

| TASK | K | | | l/s | | |
|---|---|---|---|---|---|---|
| FREQ. TYPE | L | M | N | L | M | N |
| S 1 | 6 | 6 | 6 | 6 | 6 | 6 |
| S 2 | 6 | 6 | 6 | 5 | 6 | 6 |
| S 3 | 6 | 6 | 5 | 5 | 6 | 6 |
| S 4 | 6 | 6 | 6 | 4 | 6 | 6 |
| S 5 | 6 | 6 | 6 | 6 | 6 | 6 |
| S 6 | 5 | 6 | 4 | 5 | 6 | 6 |
| TOTAL | 35 | 36 | 33 | 31 | 36 | 36 |

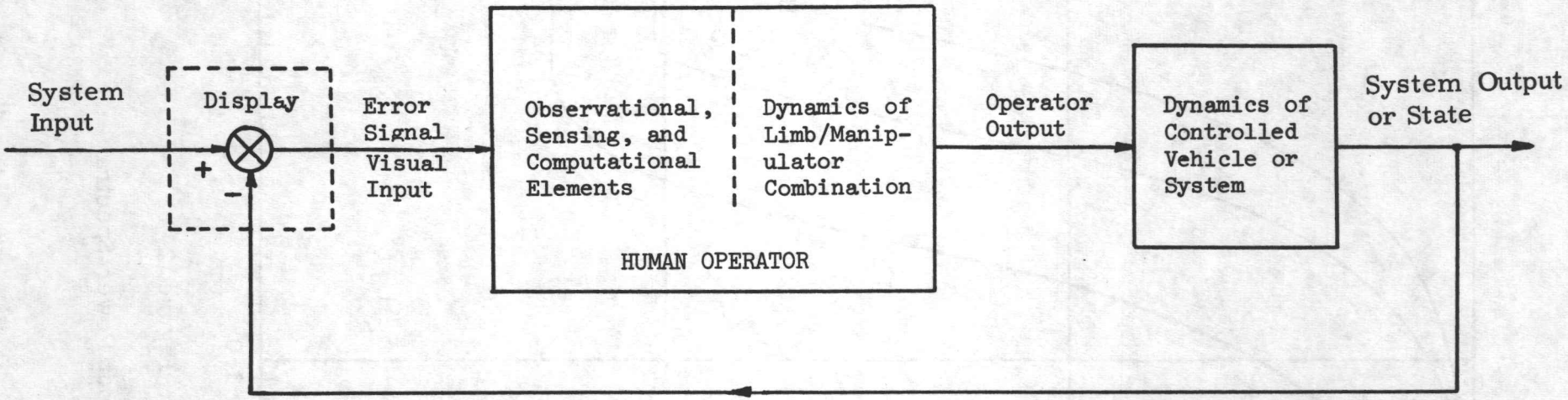


FIGURE 1. BASIC PHYSICAL SITUATION

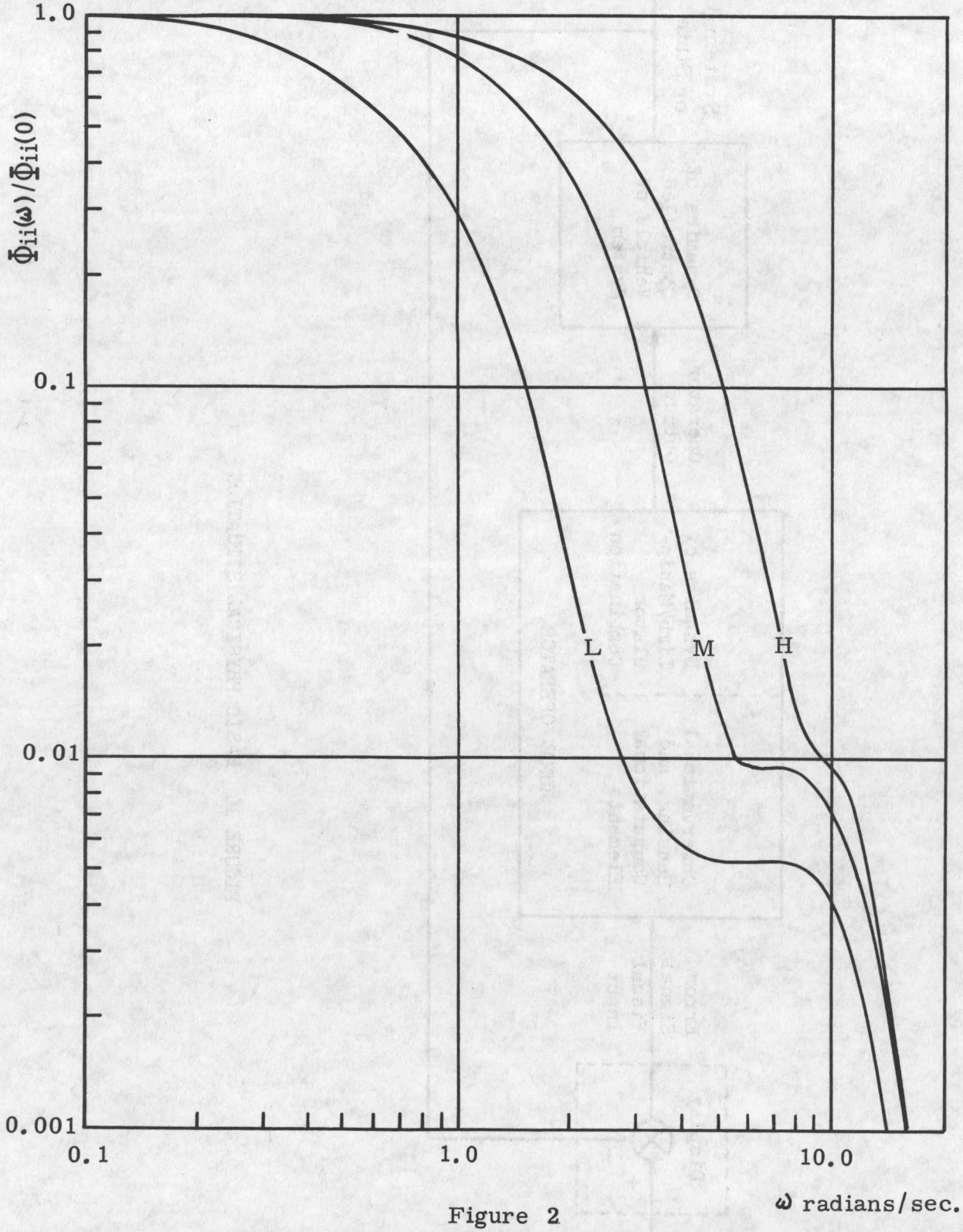


Figure 2

Input Power Spectra

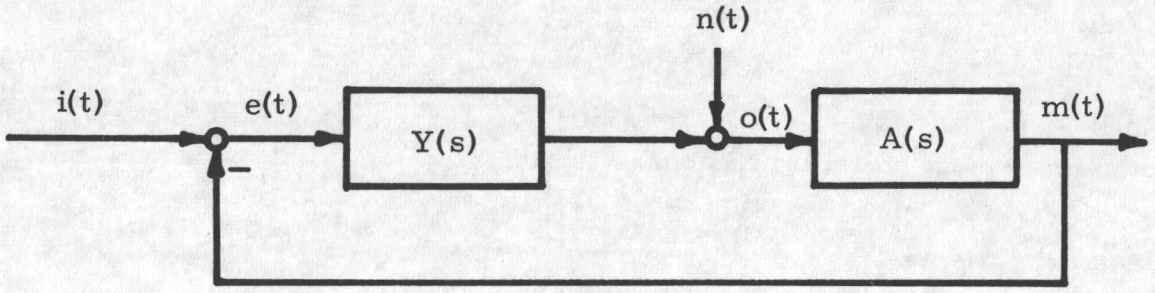


Figure 3 a Servo system for the compensatory task.

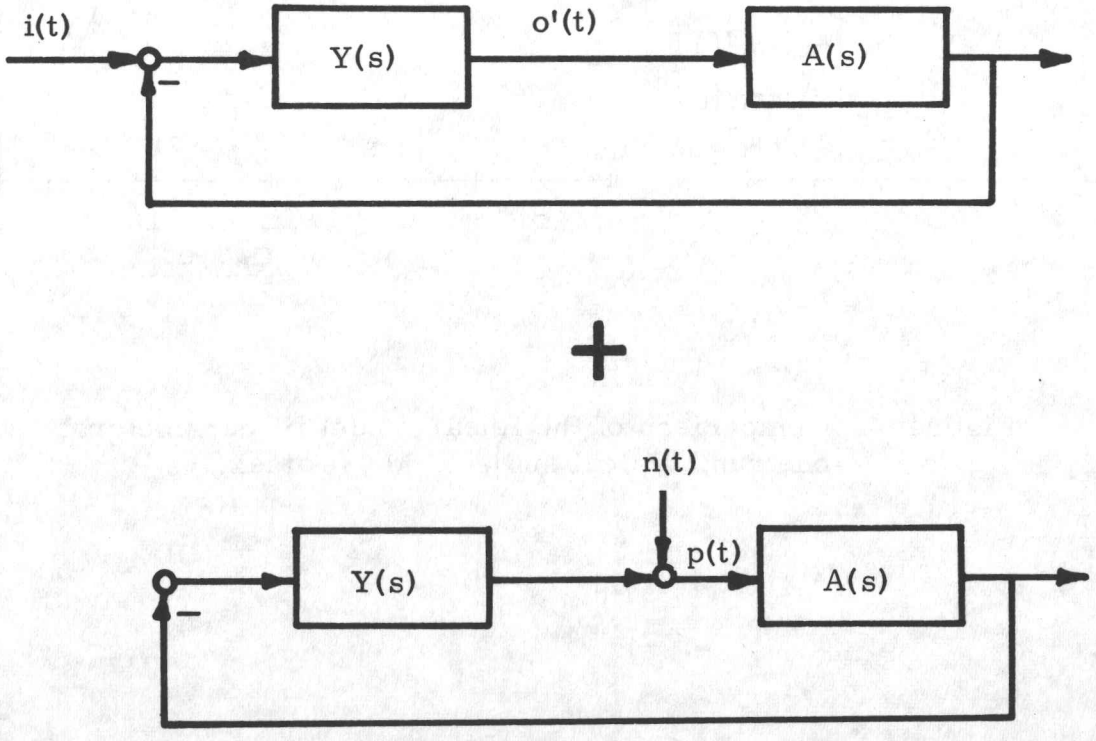


Figure 3 b Equvalent servo system

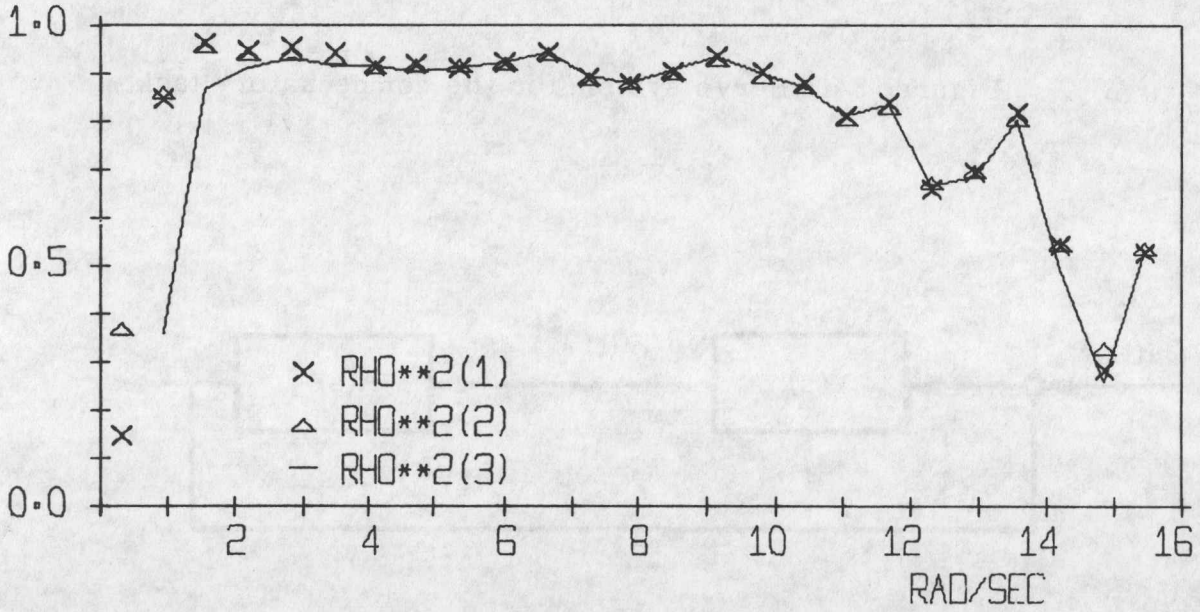


Figure 4 Comparison of the linear model fit parameters, one run, typical subject, M 1/s task.

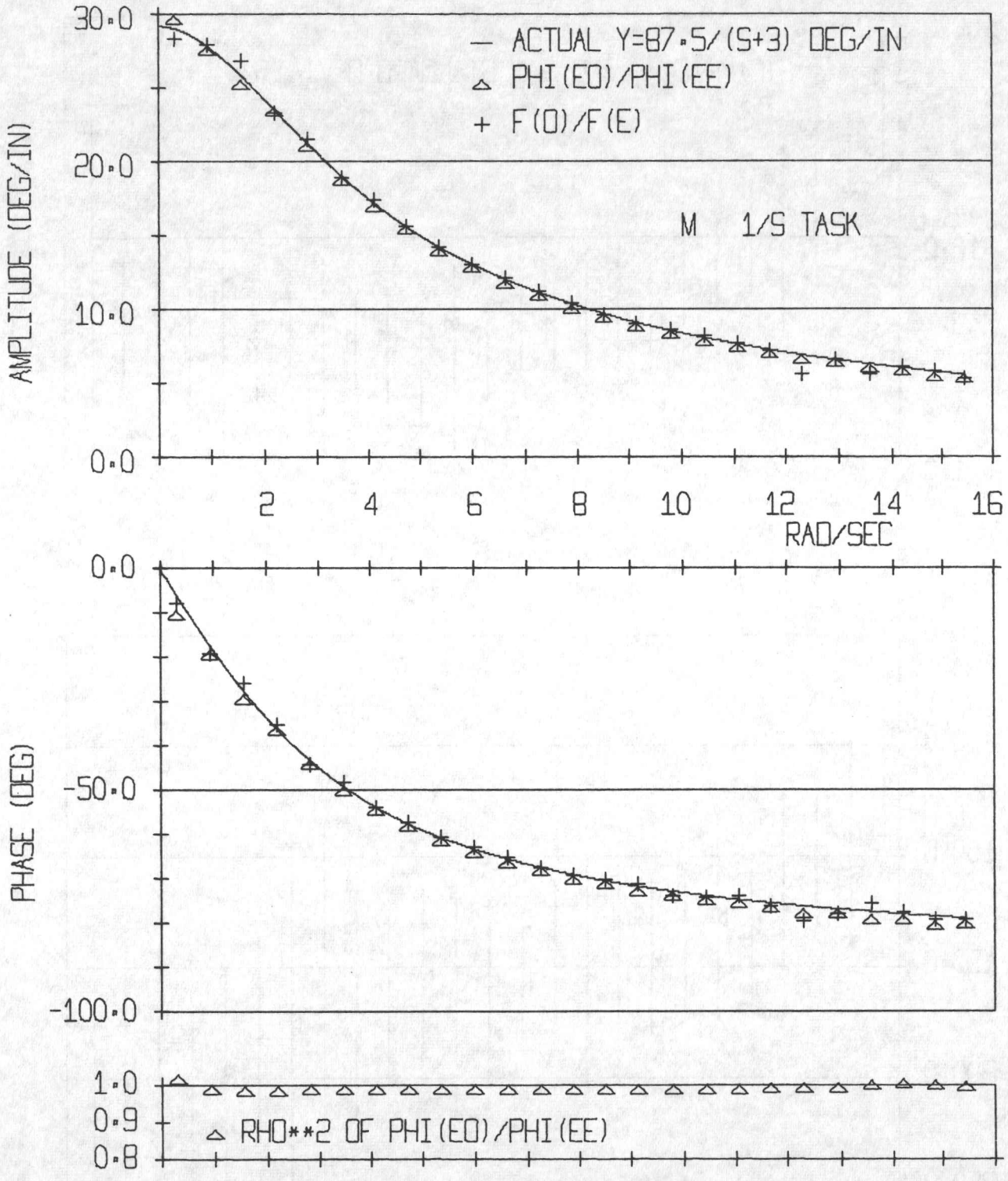


Figure 5 Analog pilot, M 1/s task.

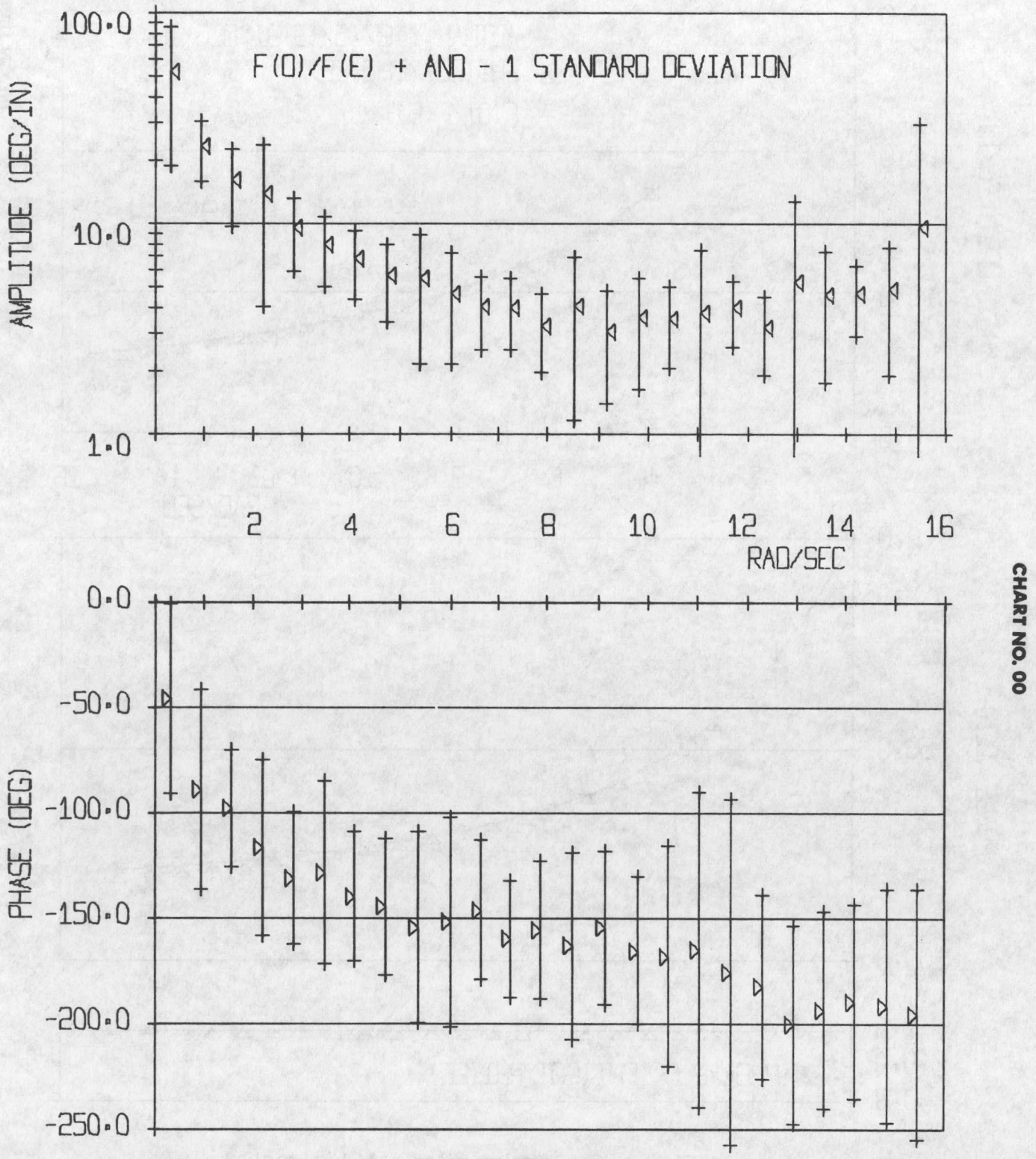


Figure 6 L K task.

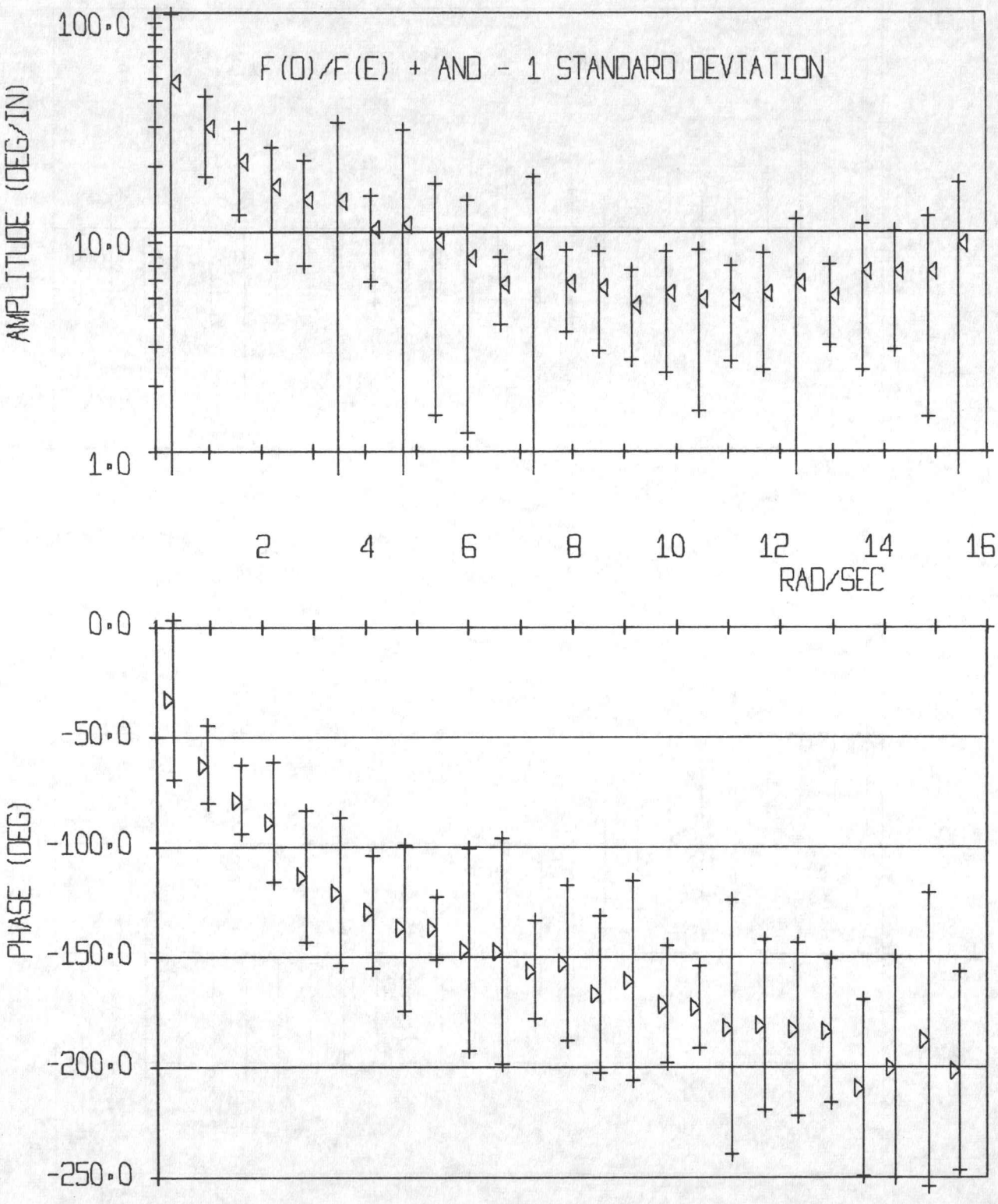


Figure 7 M K task.

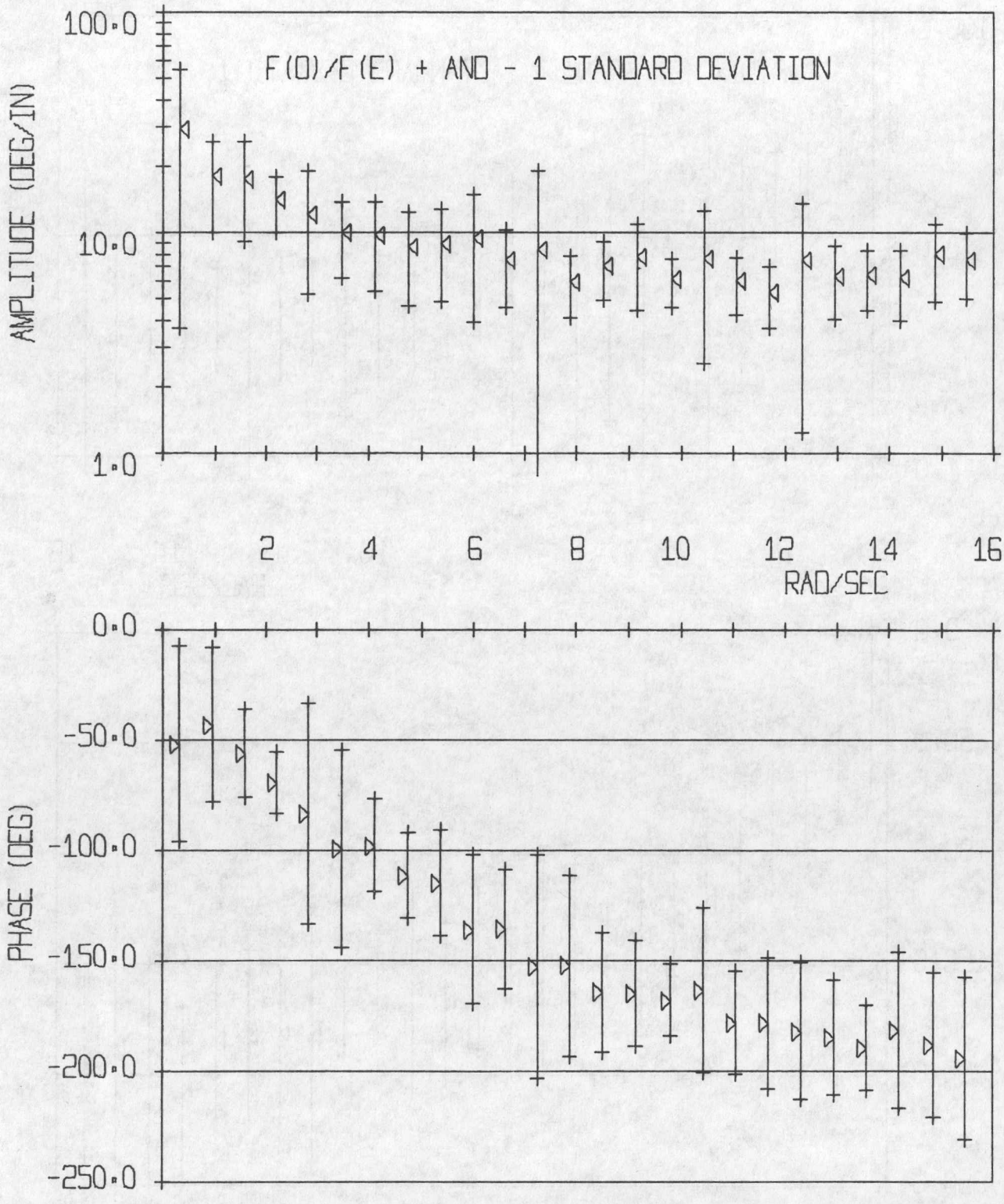


Figure 8 H K task.

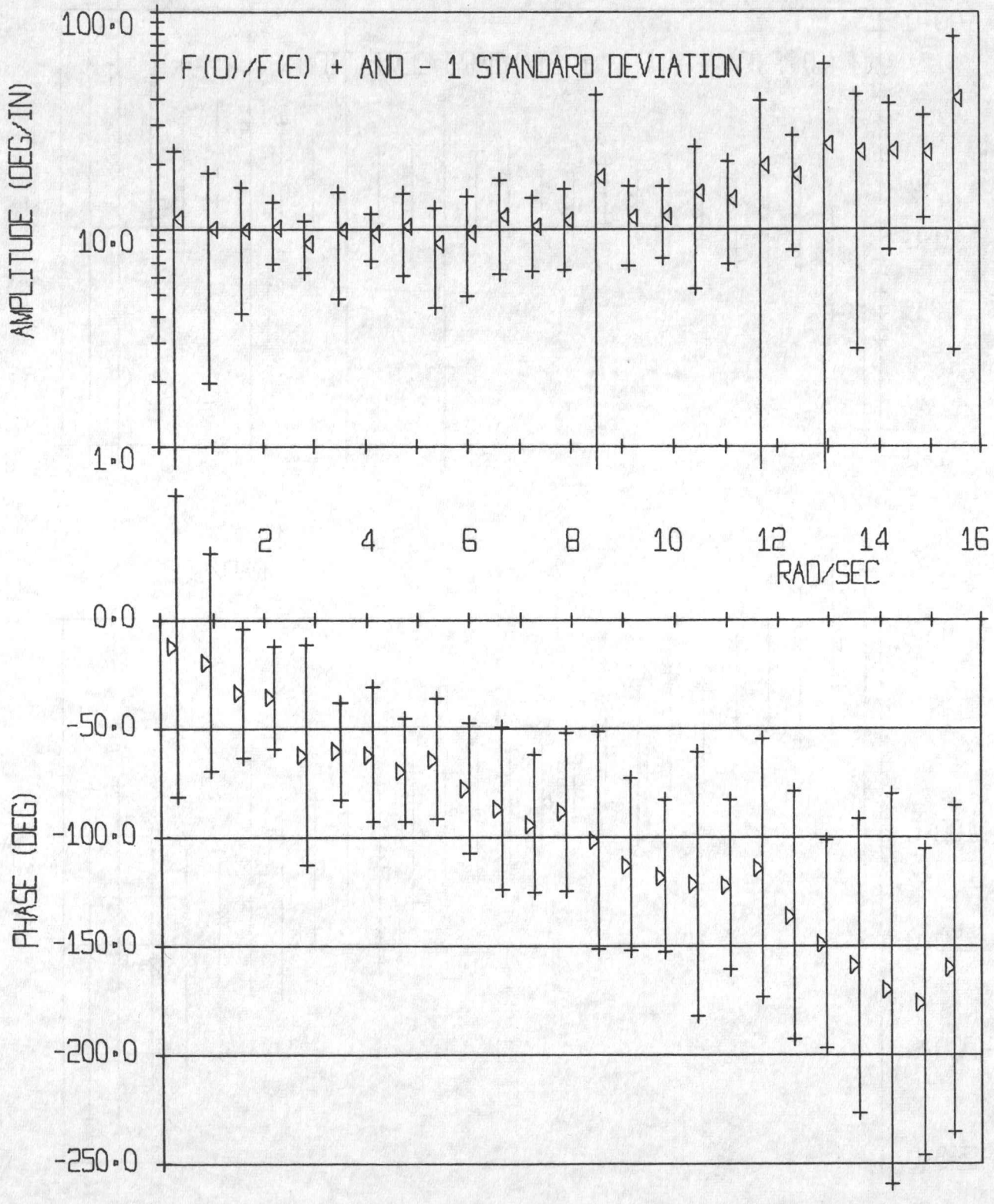


Figure 9 L 1/s task.

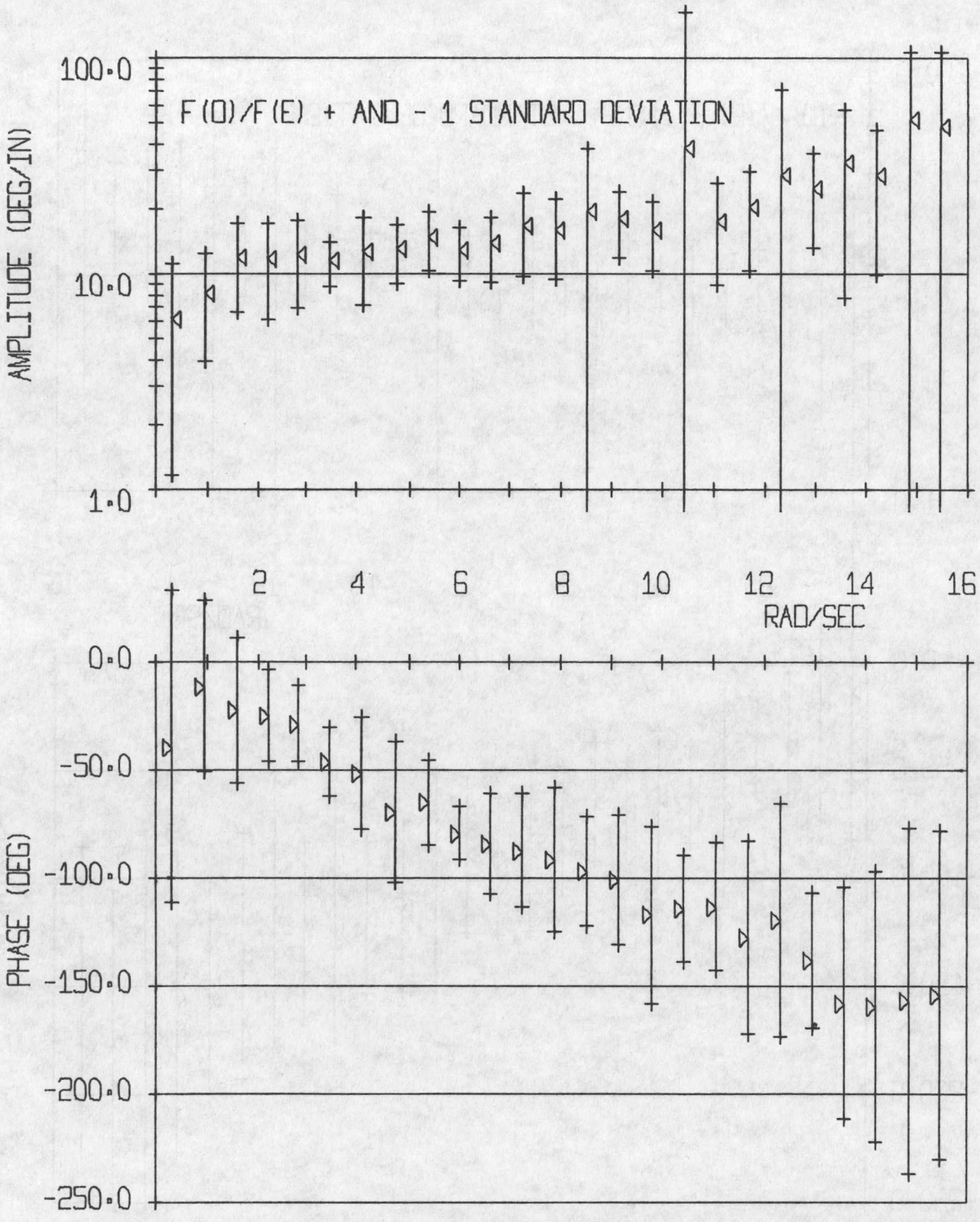


Figure 10 M 1/s task.

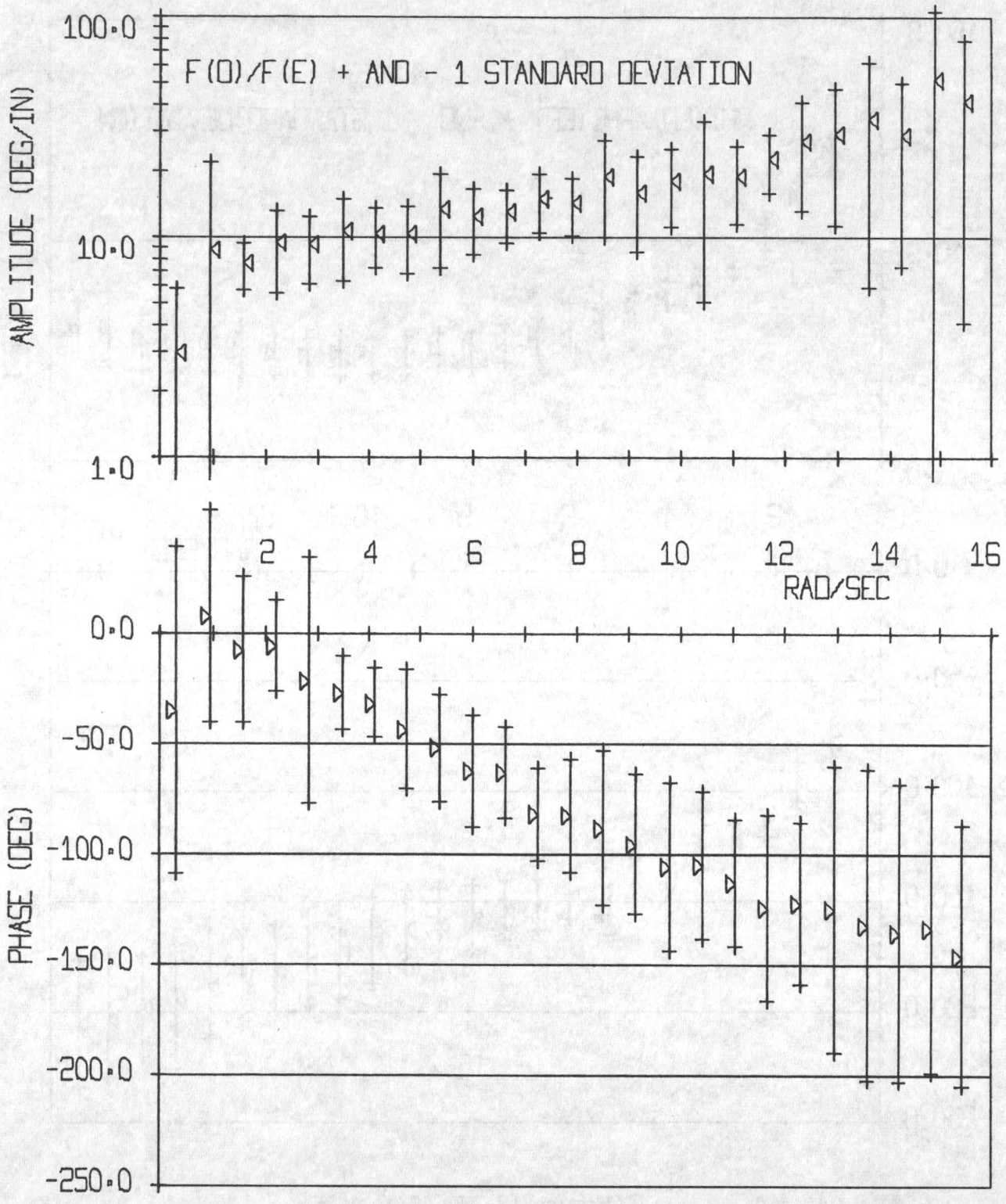


Figure 11 H 1/s task.

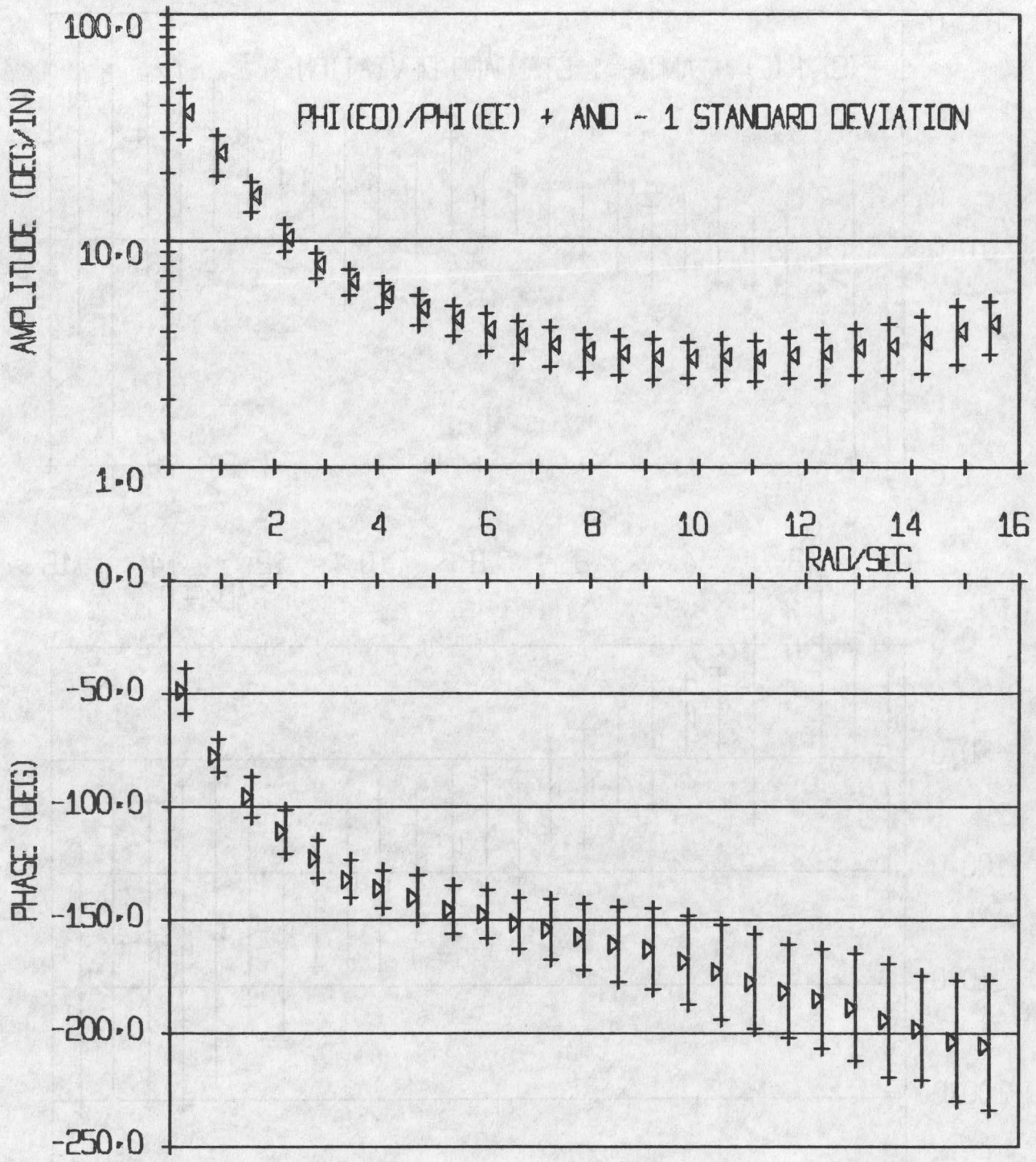


Figure 12 L K task.

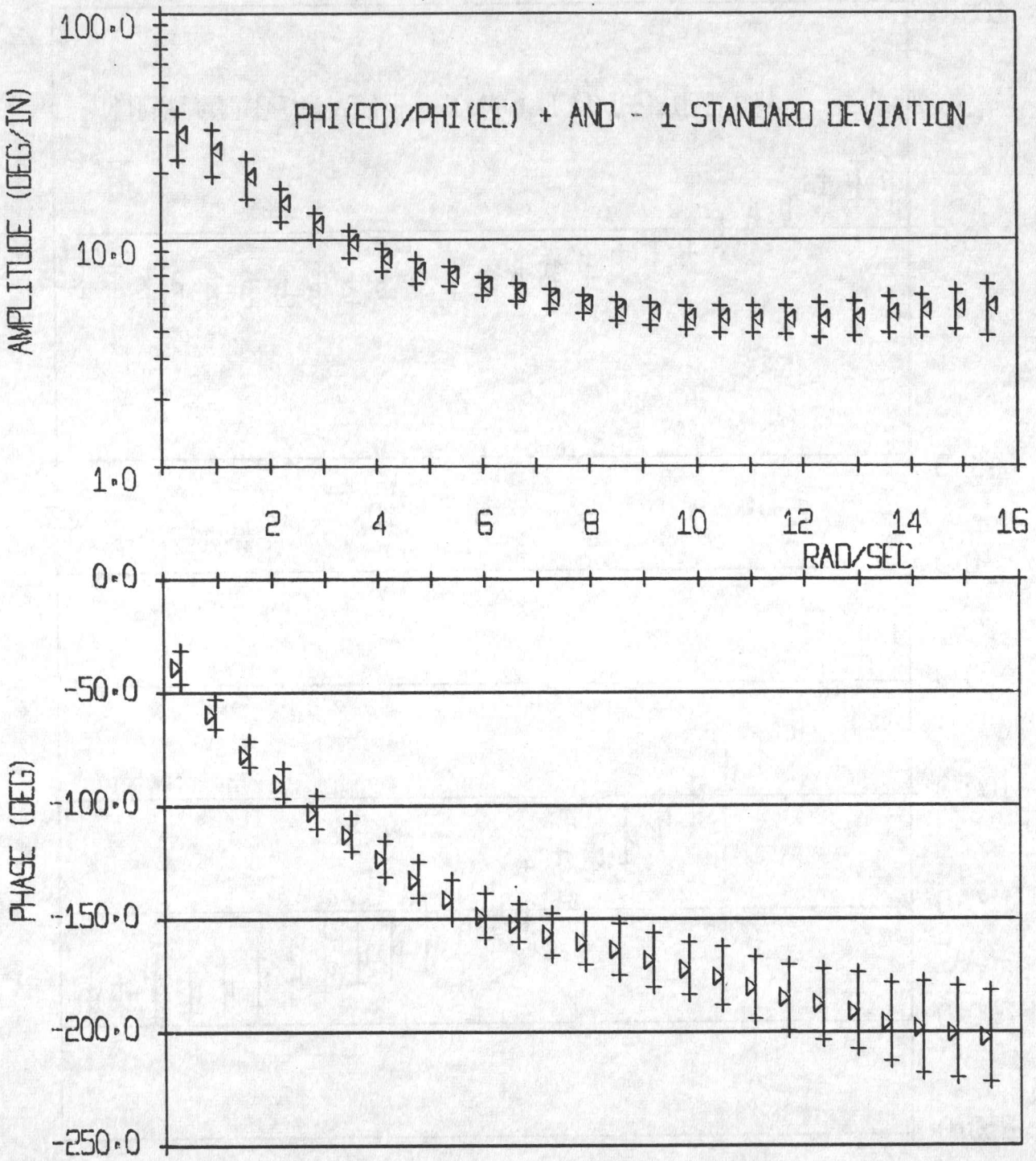


Figure 13 M K task.

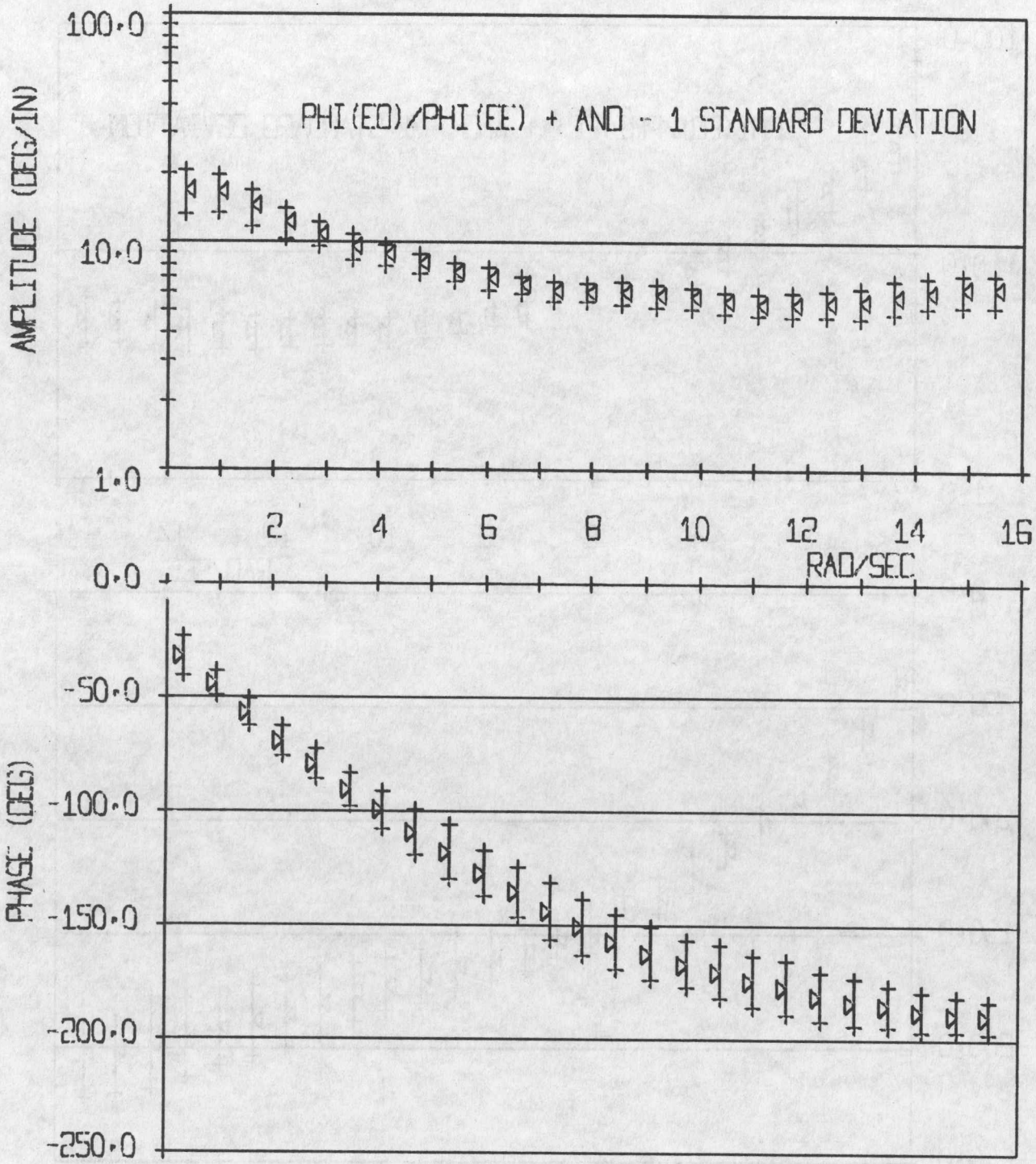


Figure 14 H K task.

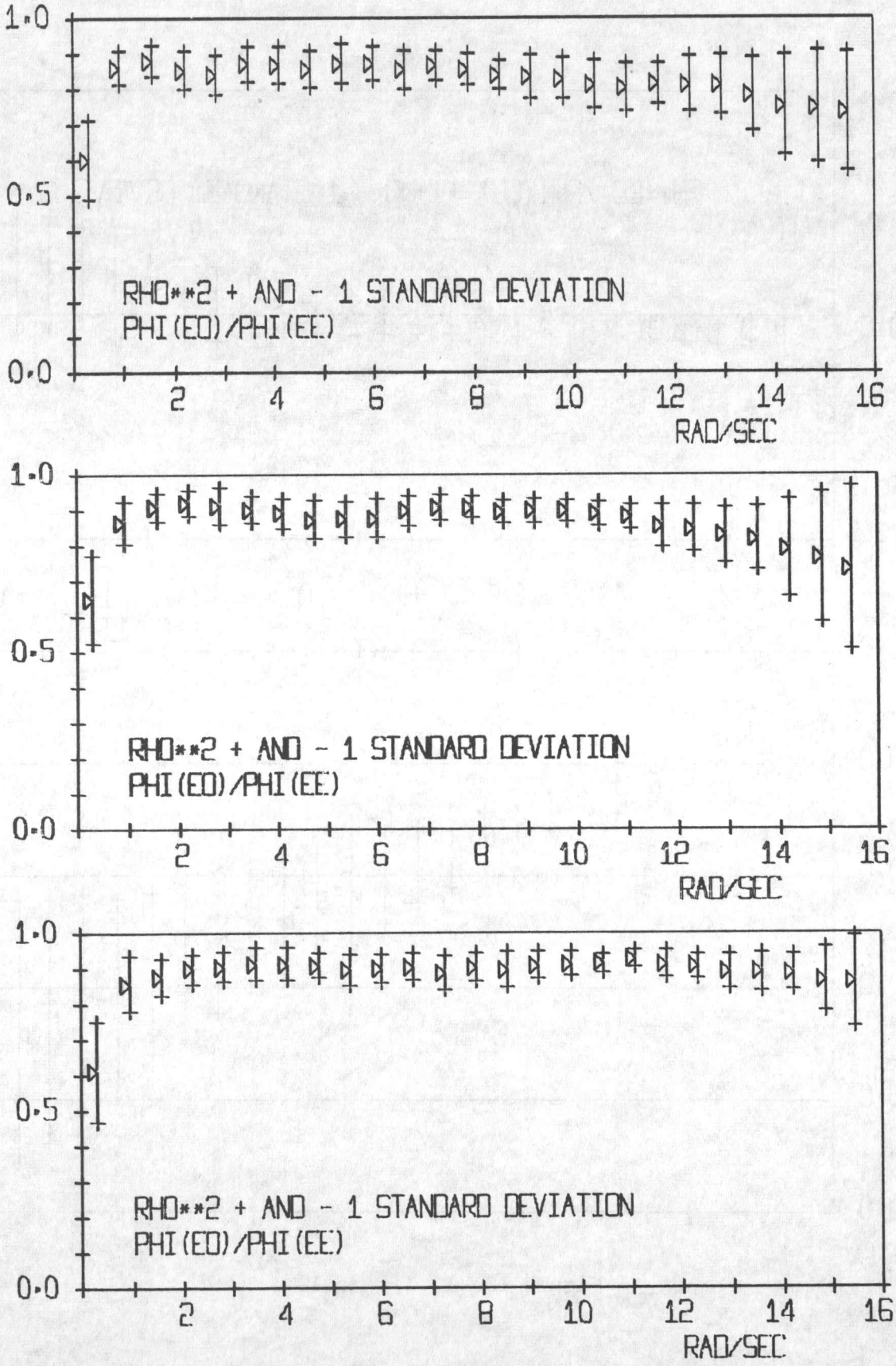


Figure 15 L K, M K, and H K task.

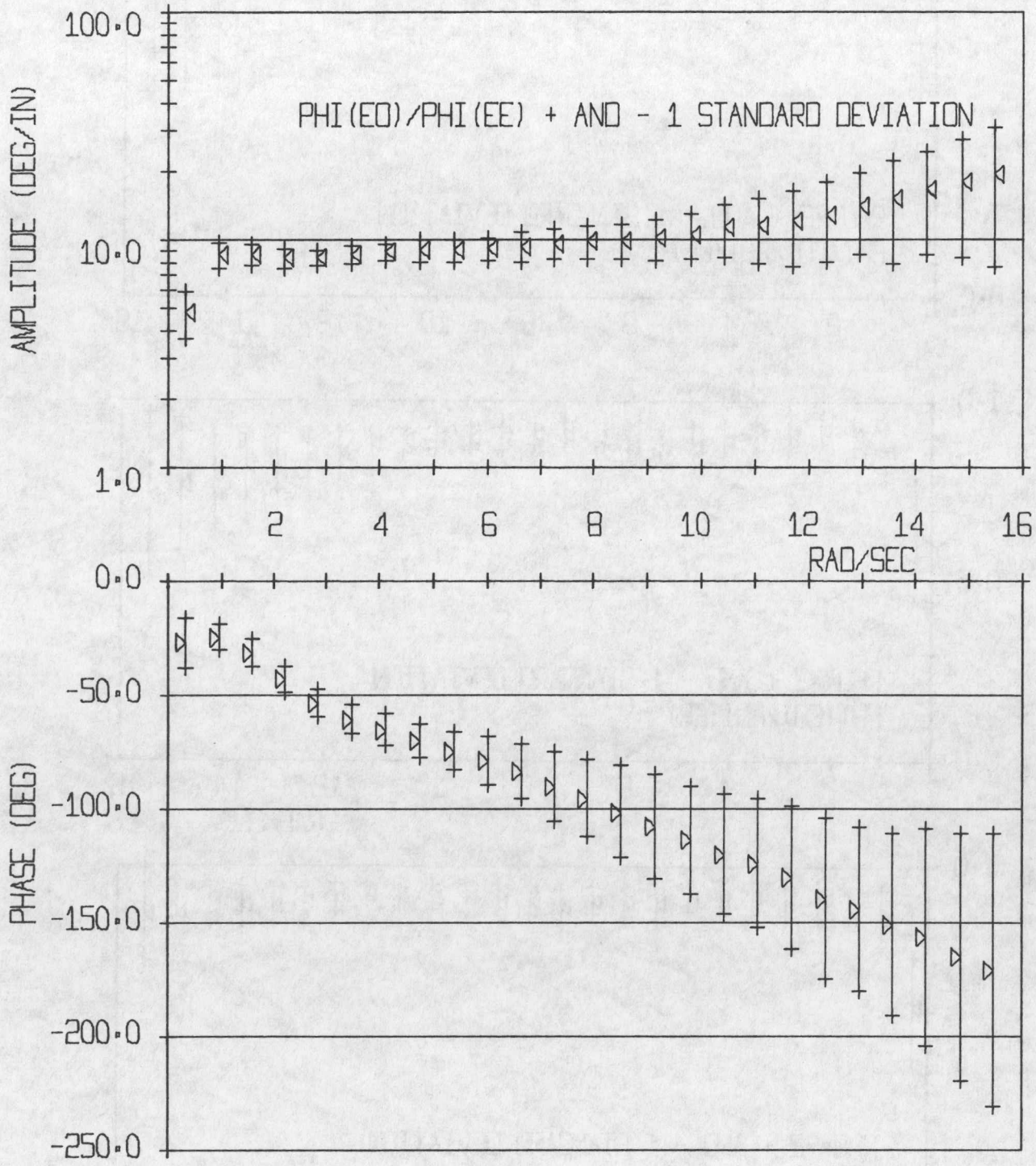


Figure 16 L 1/s task.

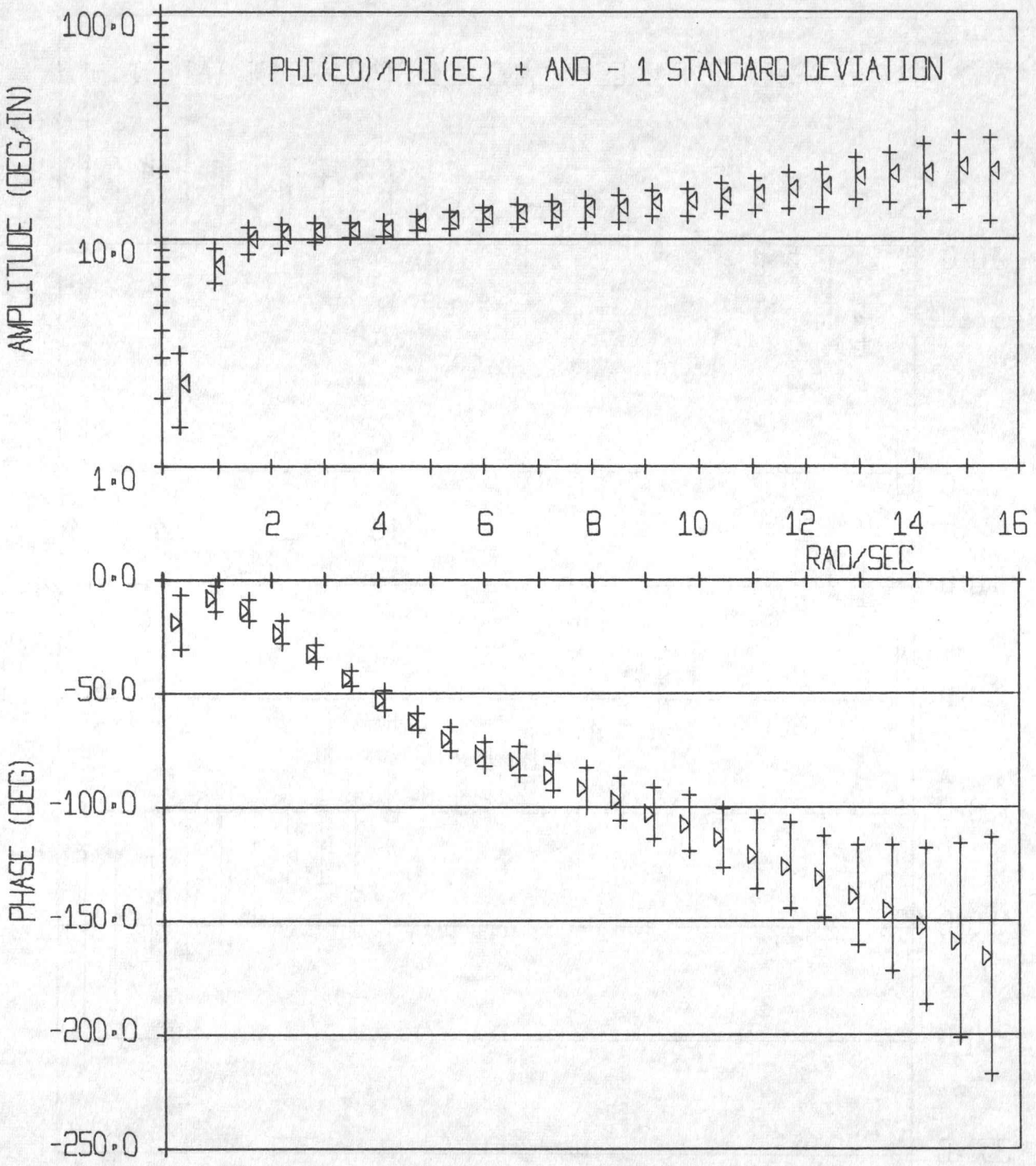


Figure 17 M 1/s task.

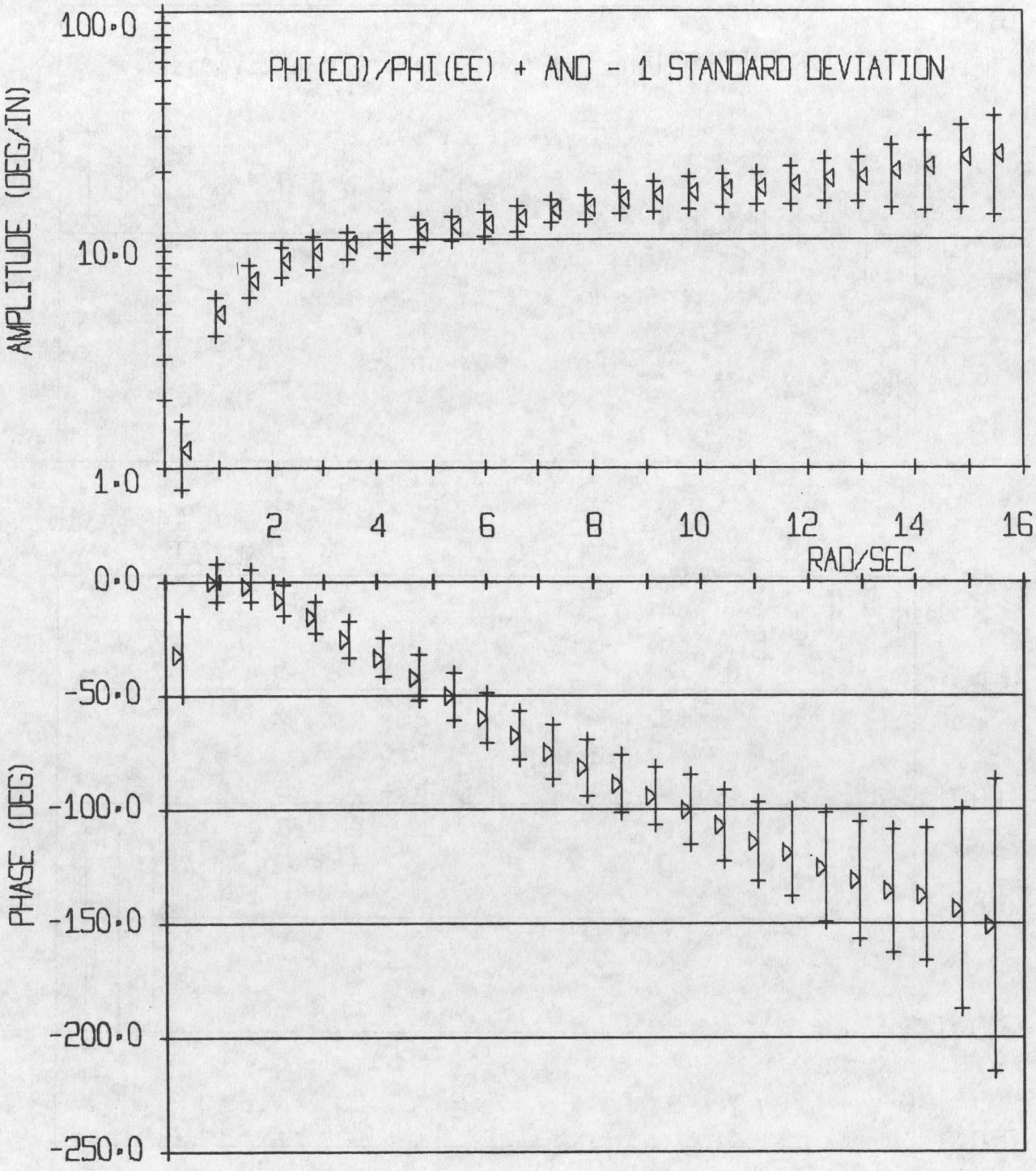


**Figure 18 H 1/s task.**

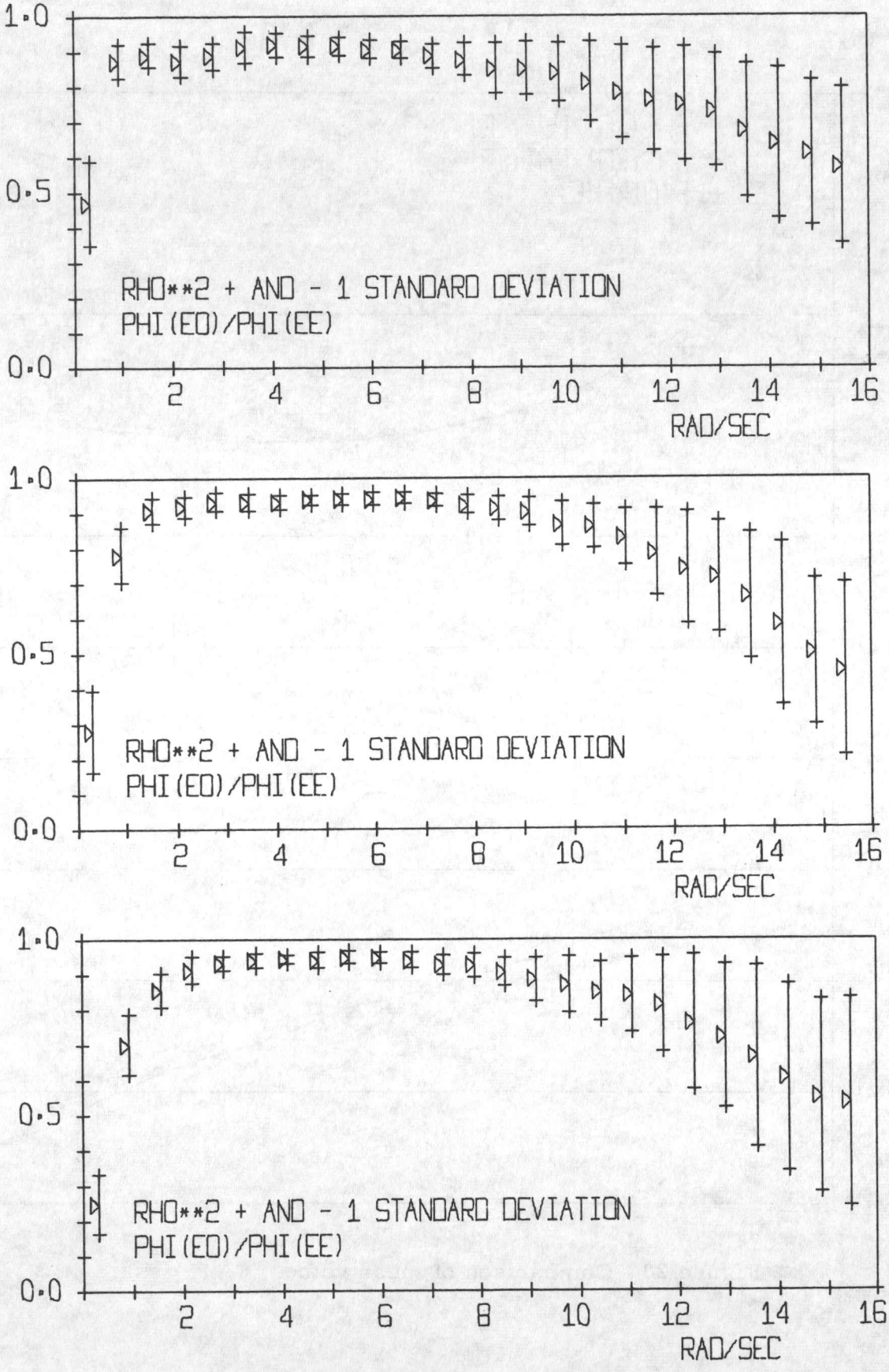


Figure 19 L 1/s, M 1/s, and H 1/s task.

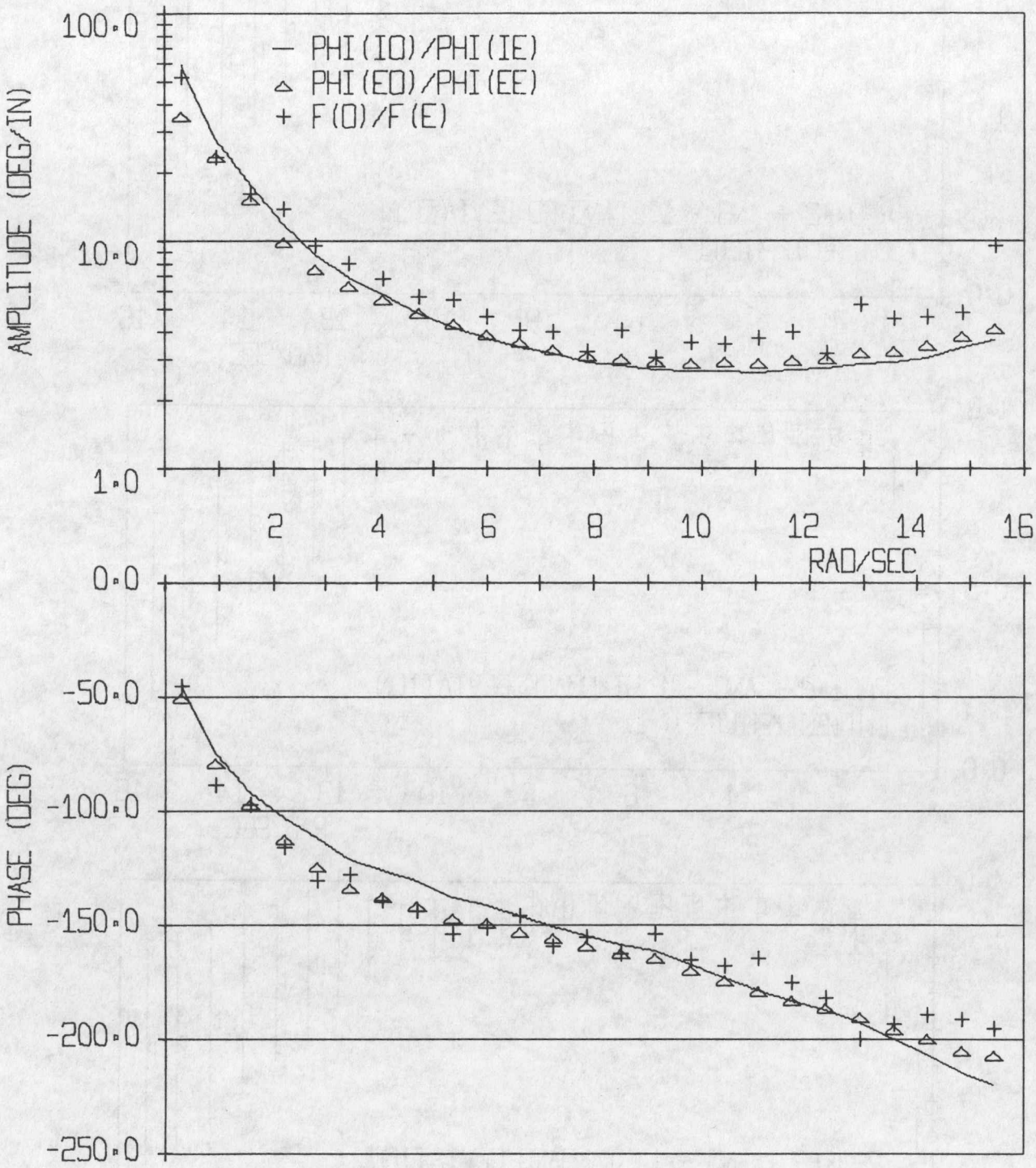


Figure 20 Comparison of mean values, L K task.

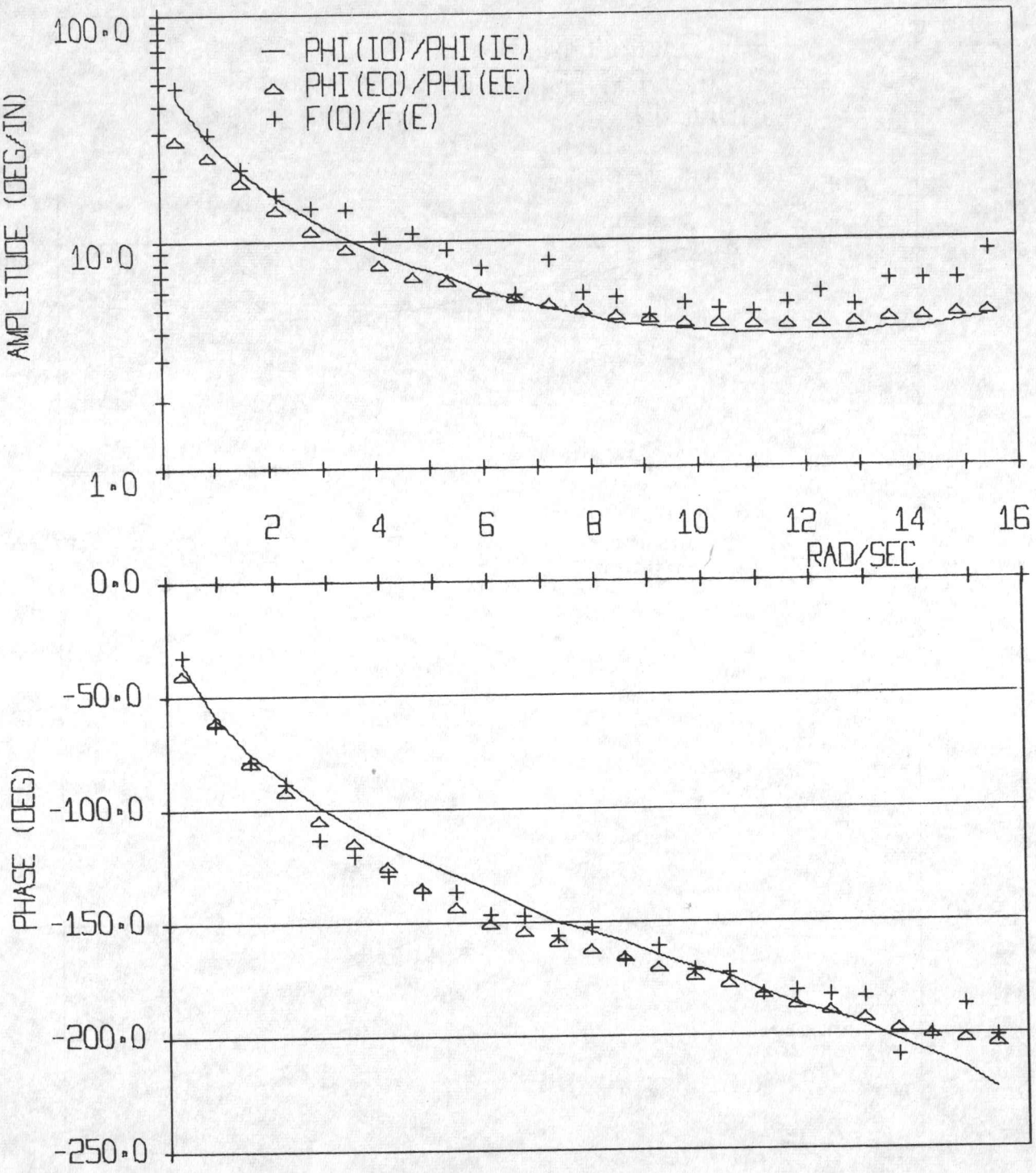


Figure 21 Comparison of mean values, M K task.

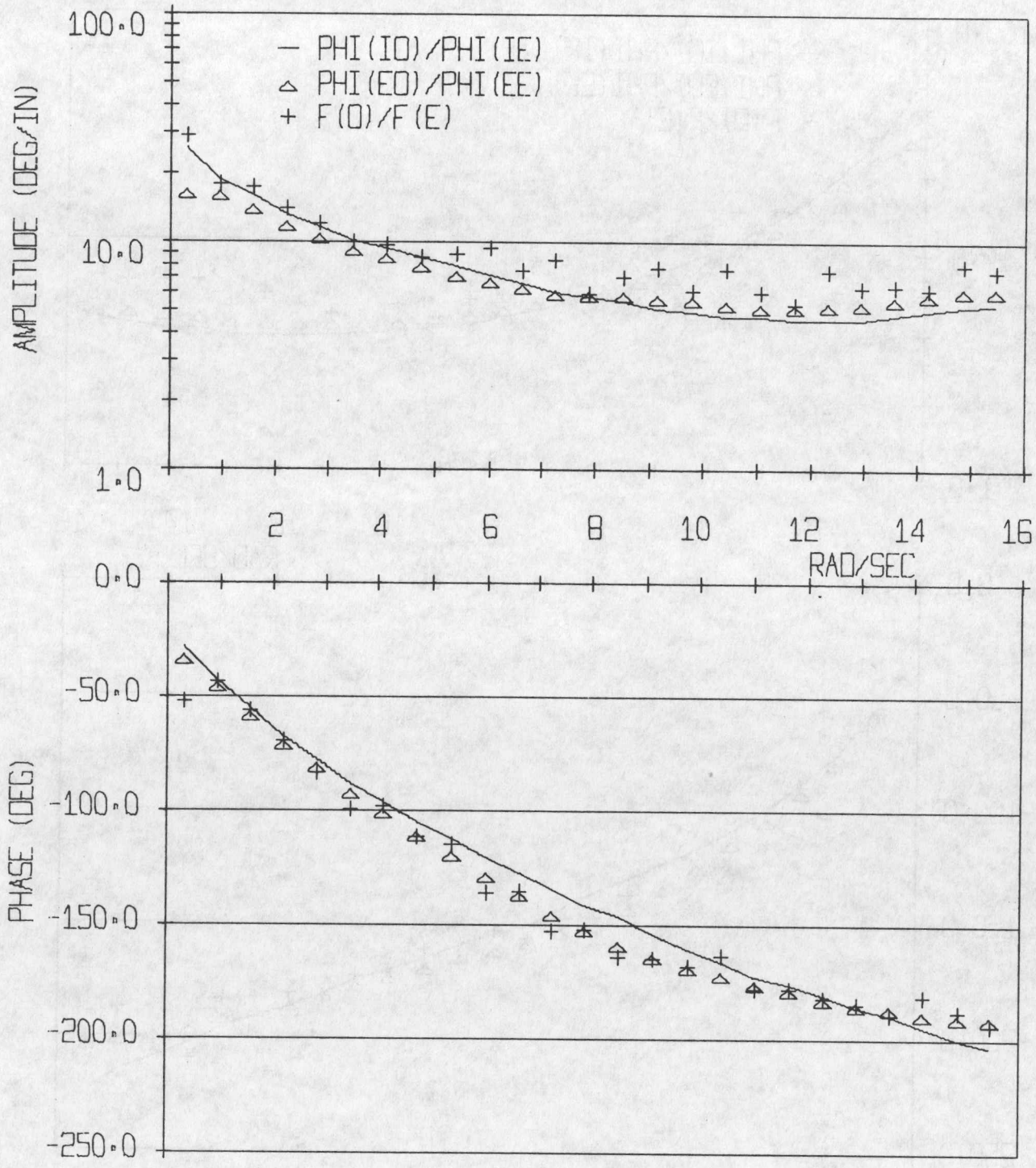


CHART NO. 00

Figure 22 Comparison of mean values, H K task.

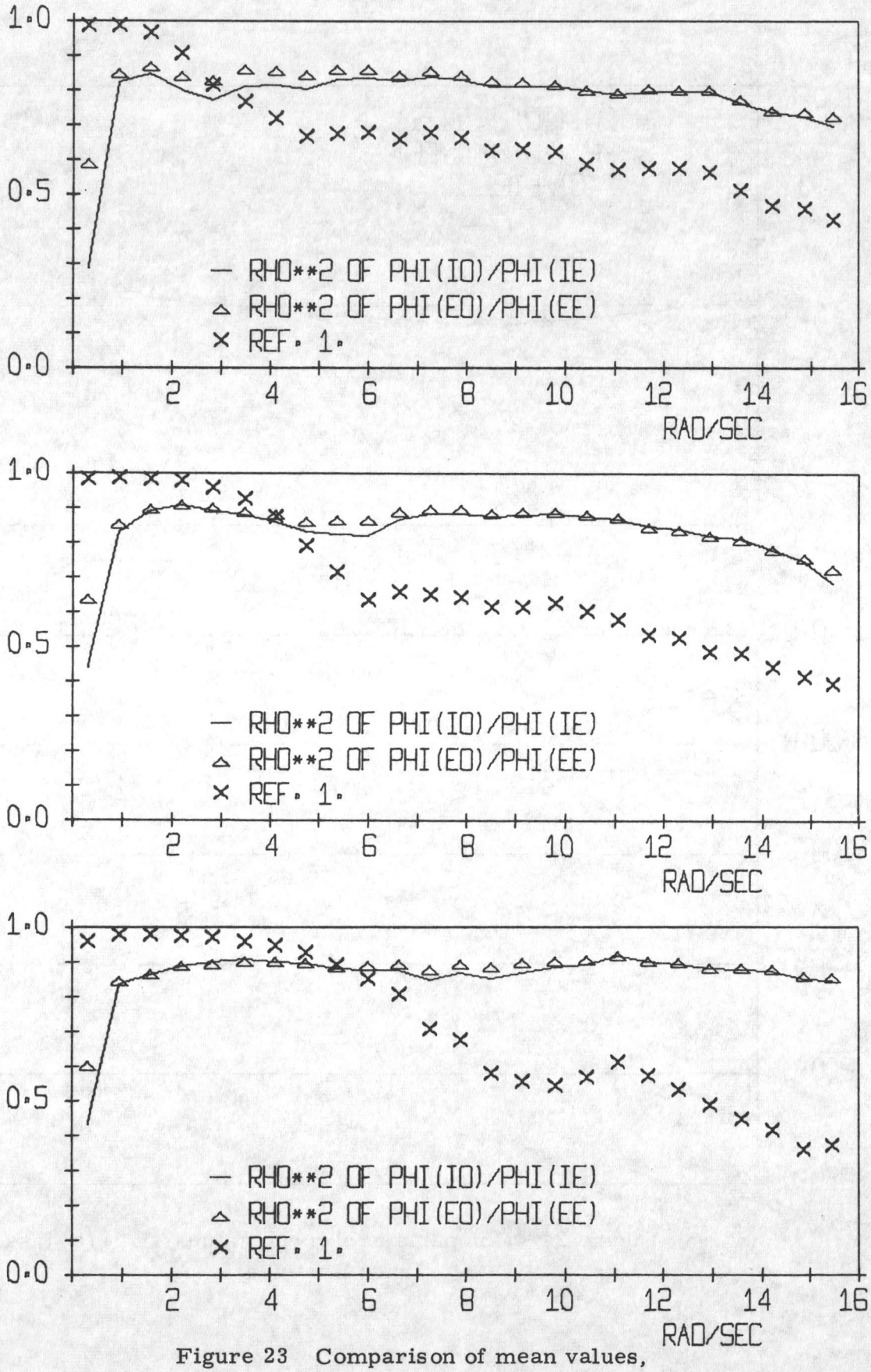


Figure 23 Comparison of mean values,

L K, M K, and H K task.

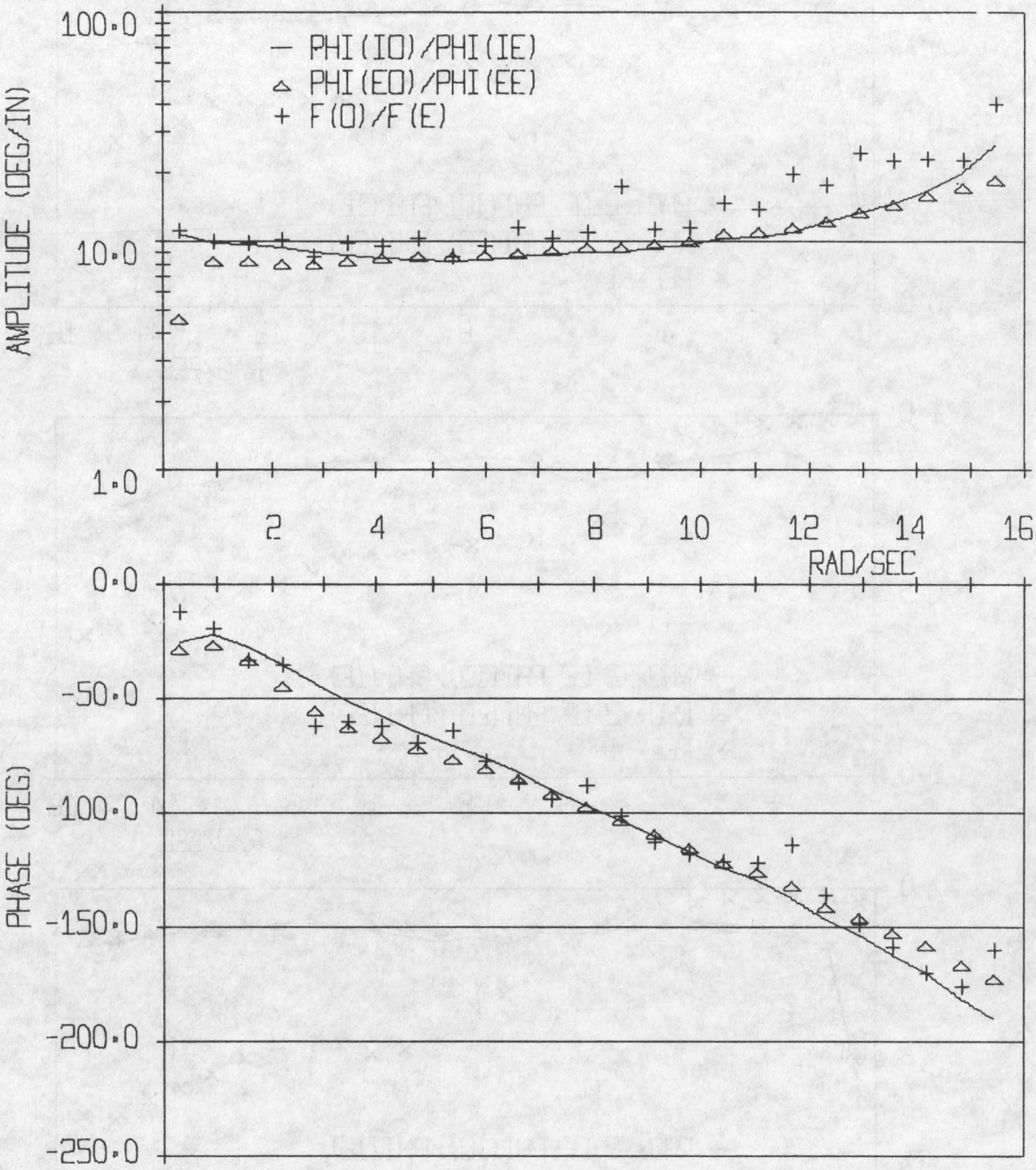


Figure 24 Comparison of mean values, L 1/s task.

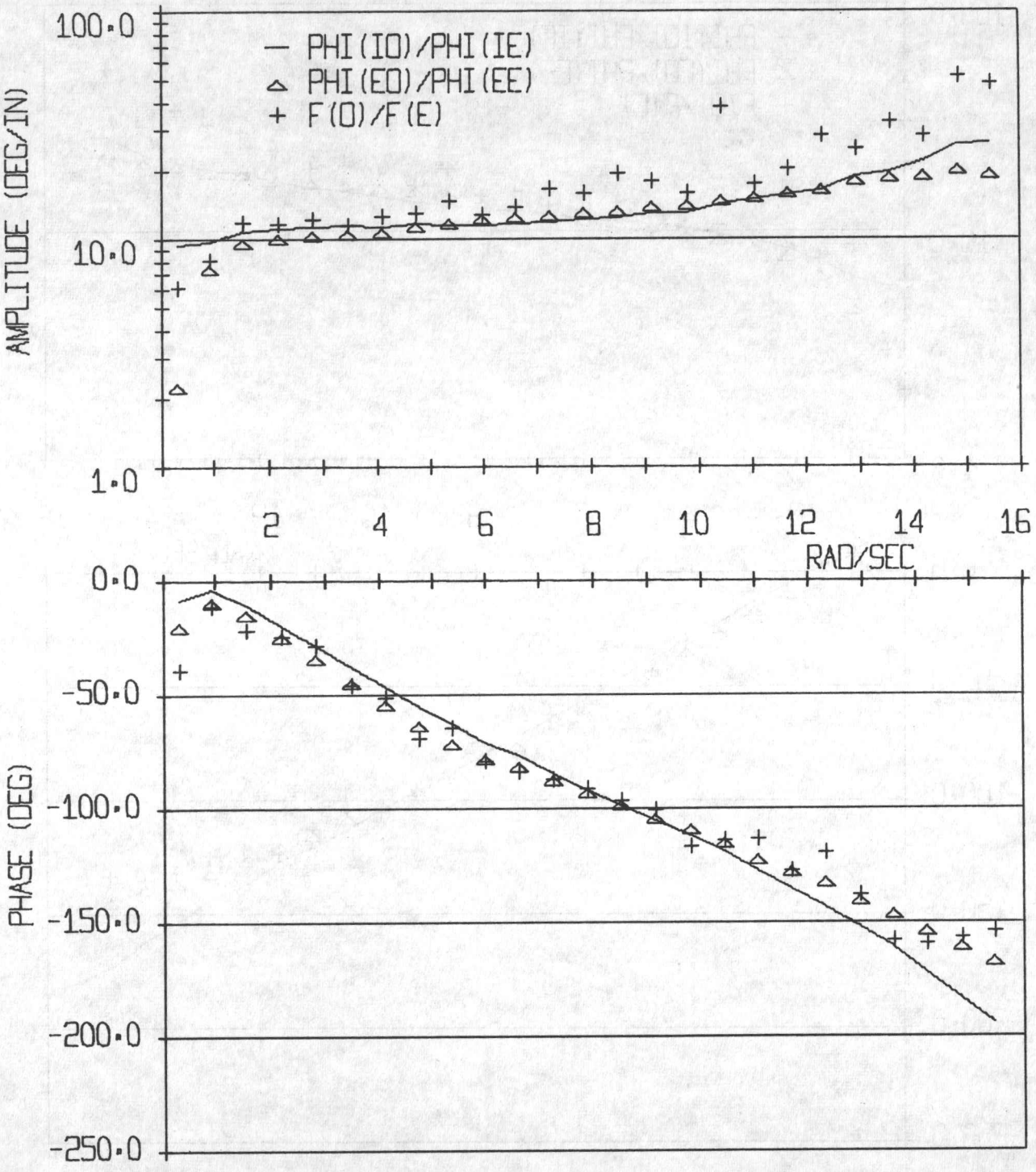


Figure 25 Comparison of mean values, M 1/s task.

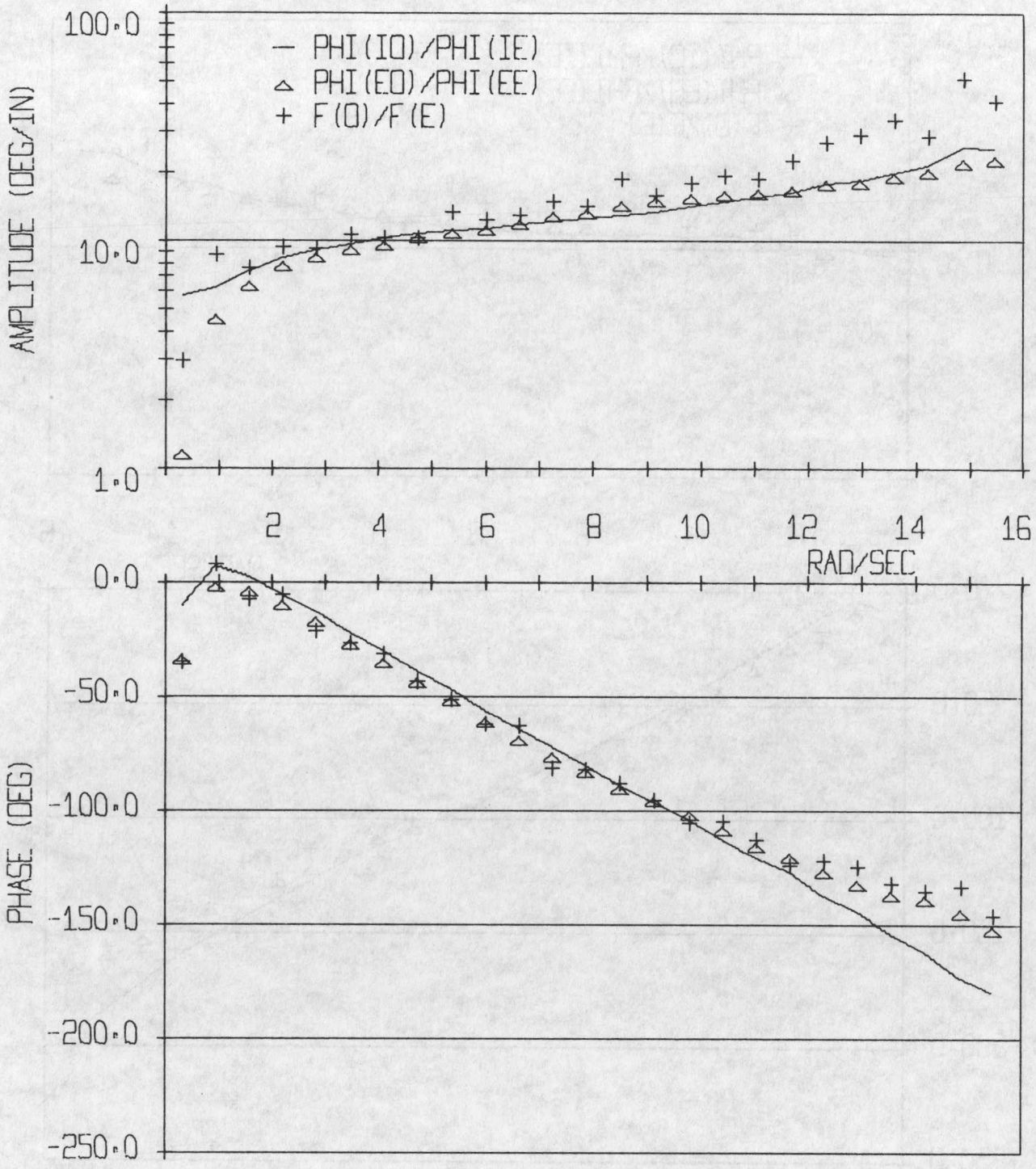


Figure 26 Comparison of mean values, H 1/s task.

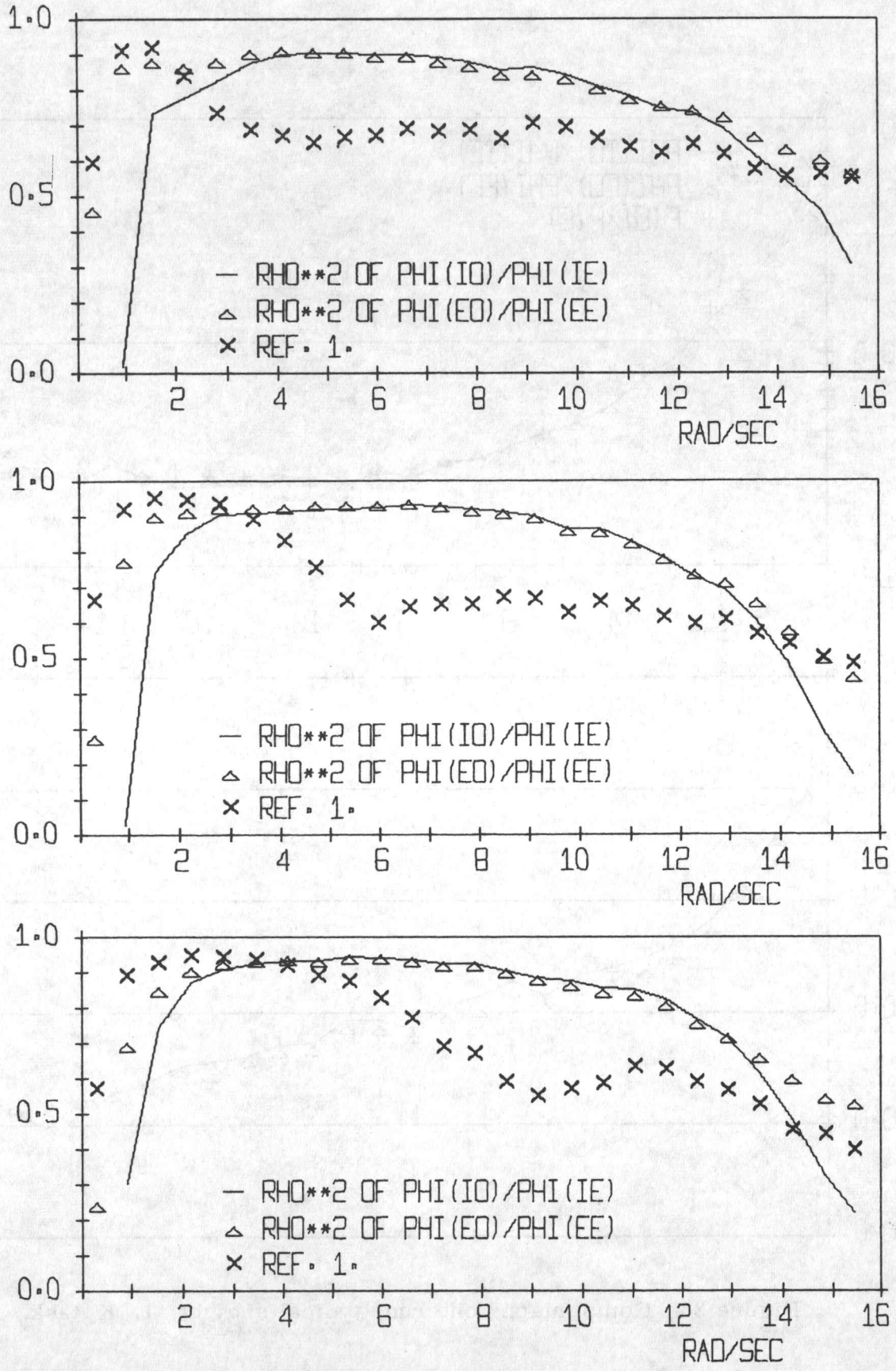


Figure 27 Comparison of mean values,

L 1/s, M 1/s, and H 1/s task.

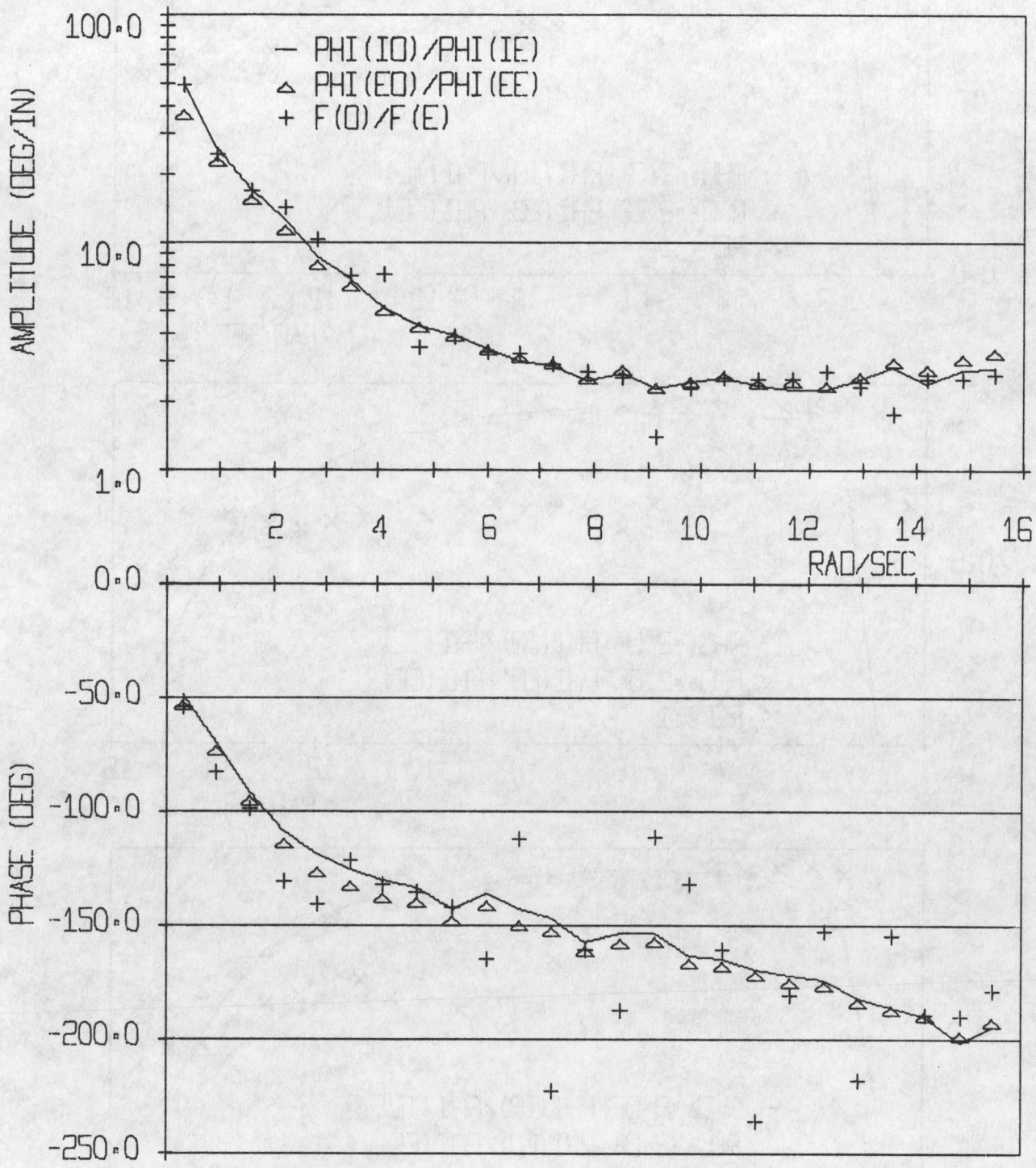


Figure 28 Comparison, one run, typical subject, L K task.

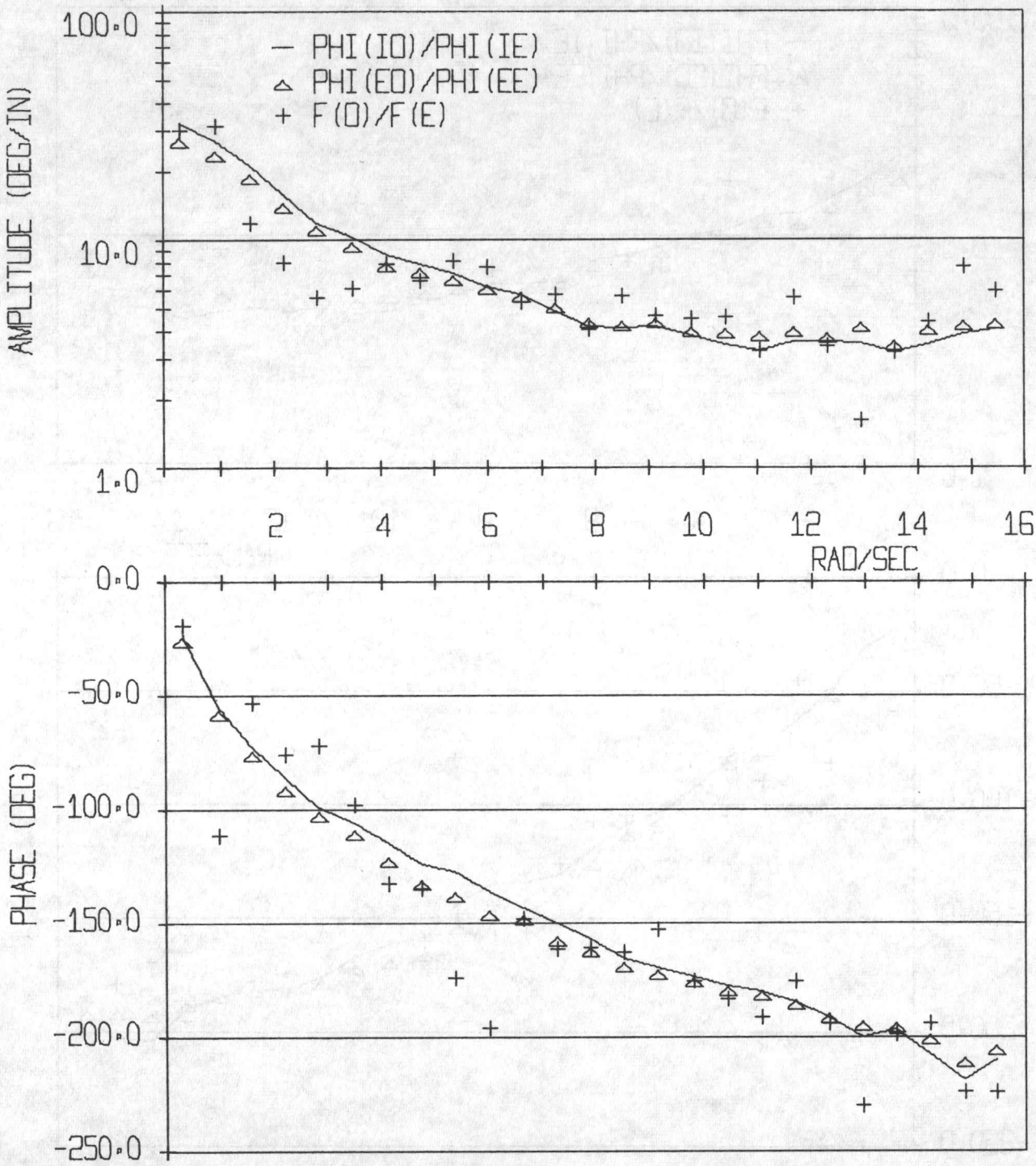


Figure 29 Comparison, one run, typical subject, M K task.

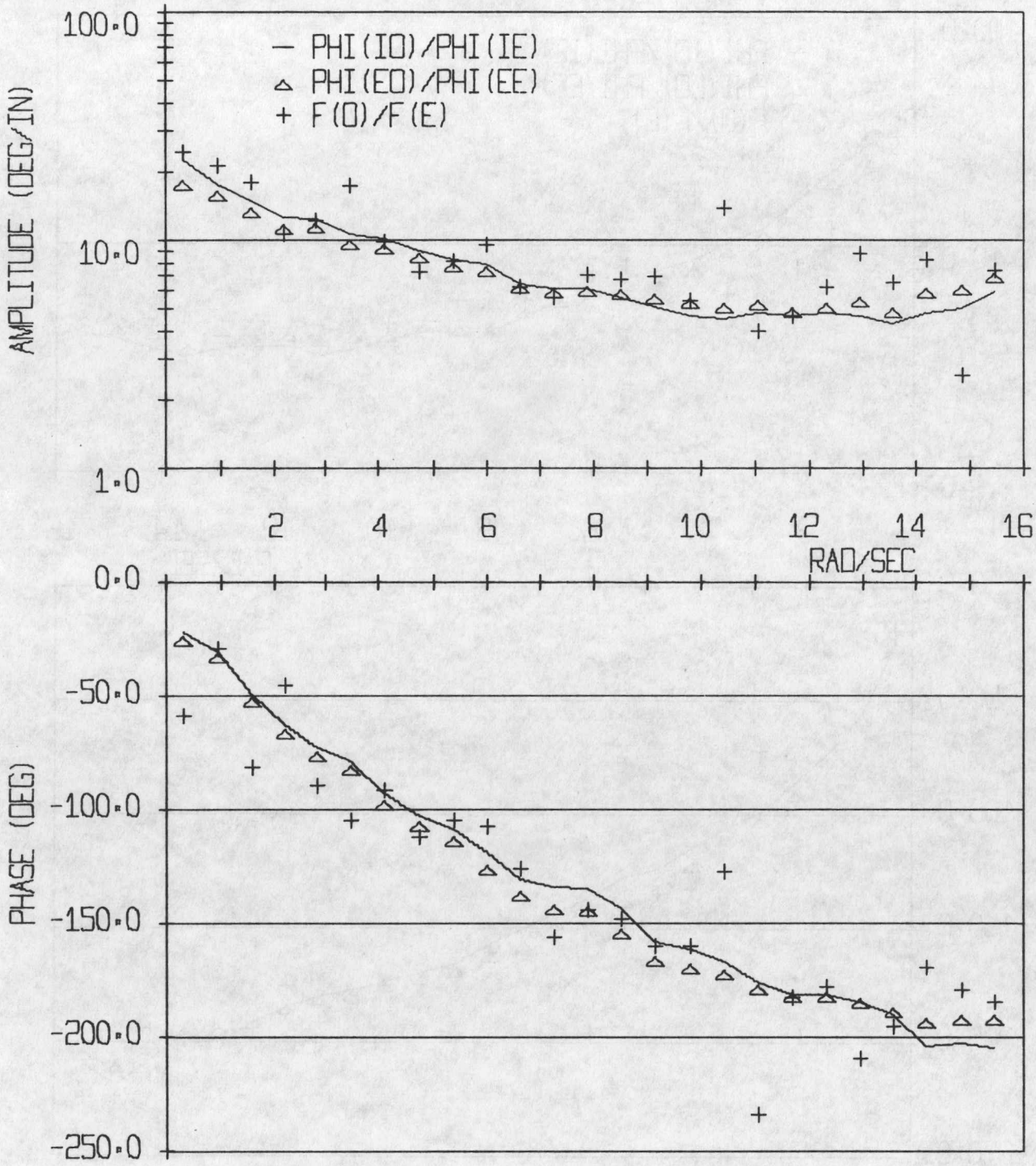


Figure 30 Comparison, one run, typical subject, H K task.

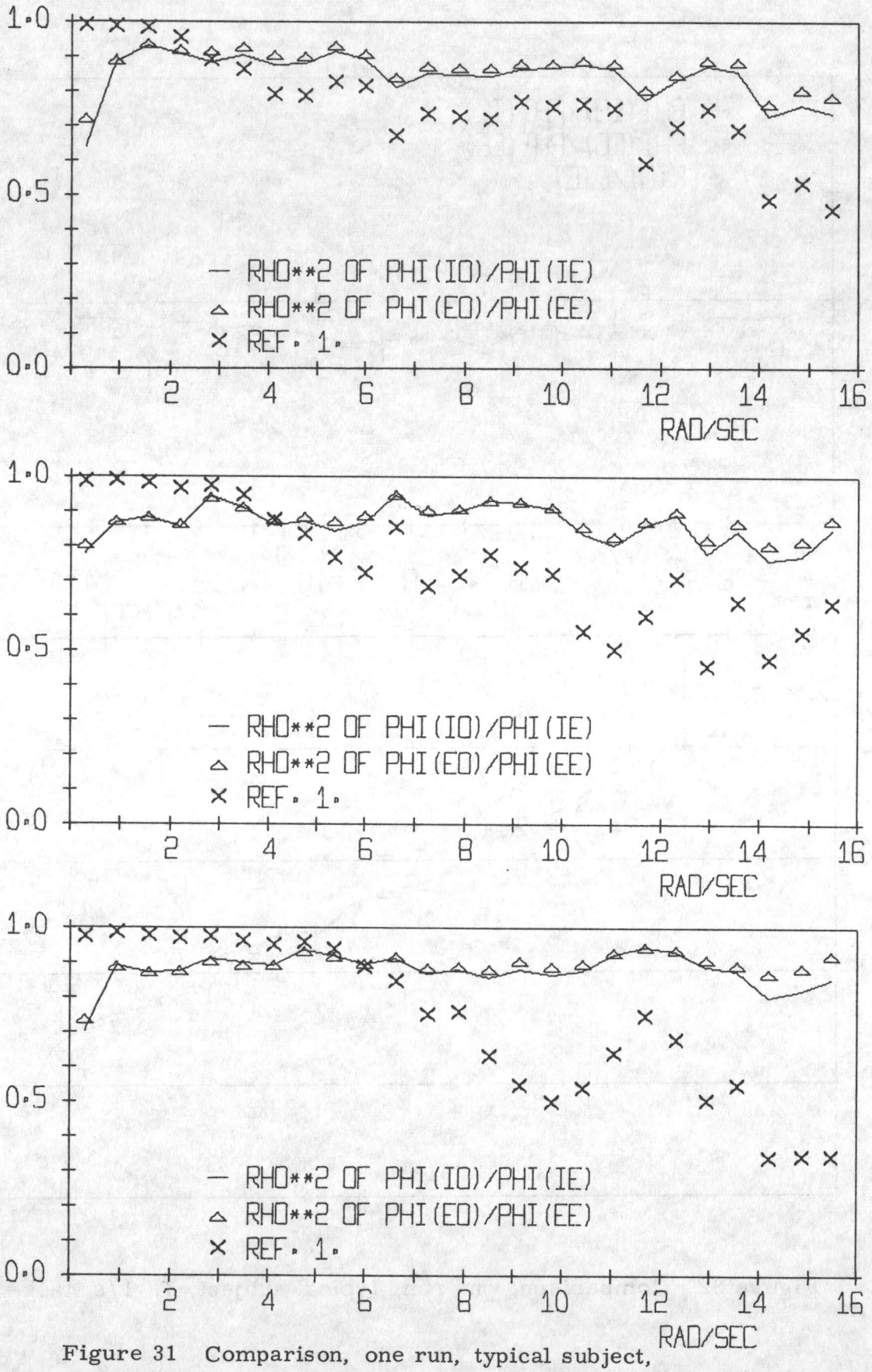


Figure 31 Comparison, one run, typical subject,

L K, M K, and H K task.

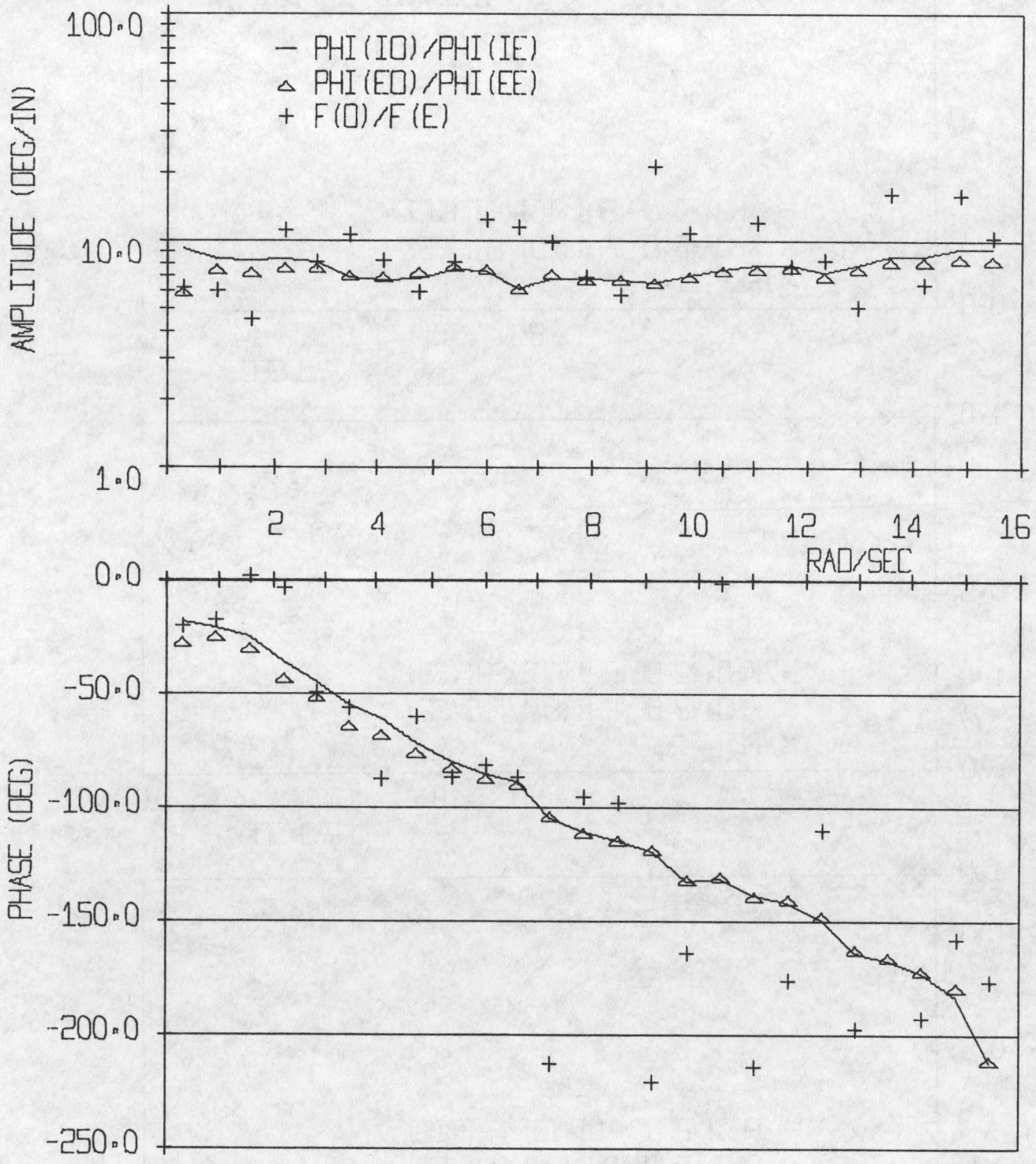


Figure 32 Comparison, one run, typical subject, L 1/s task.

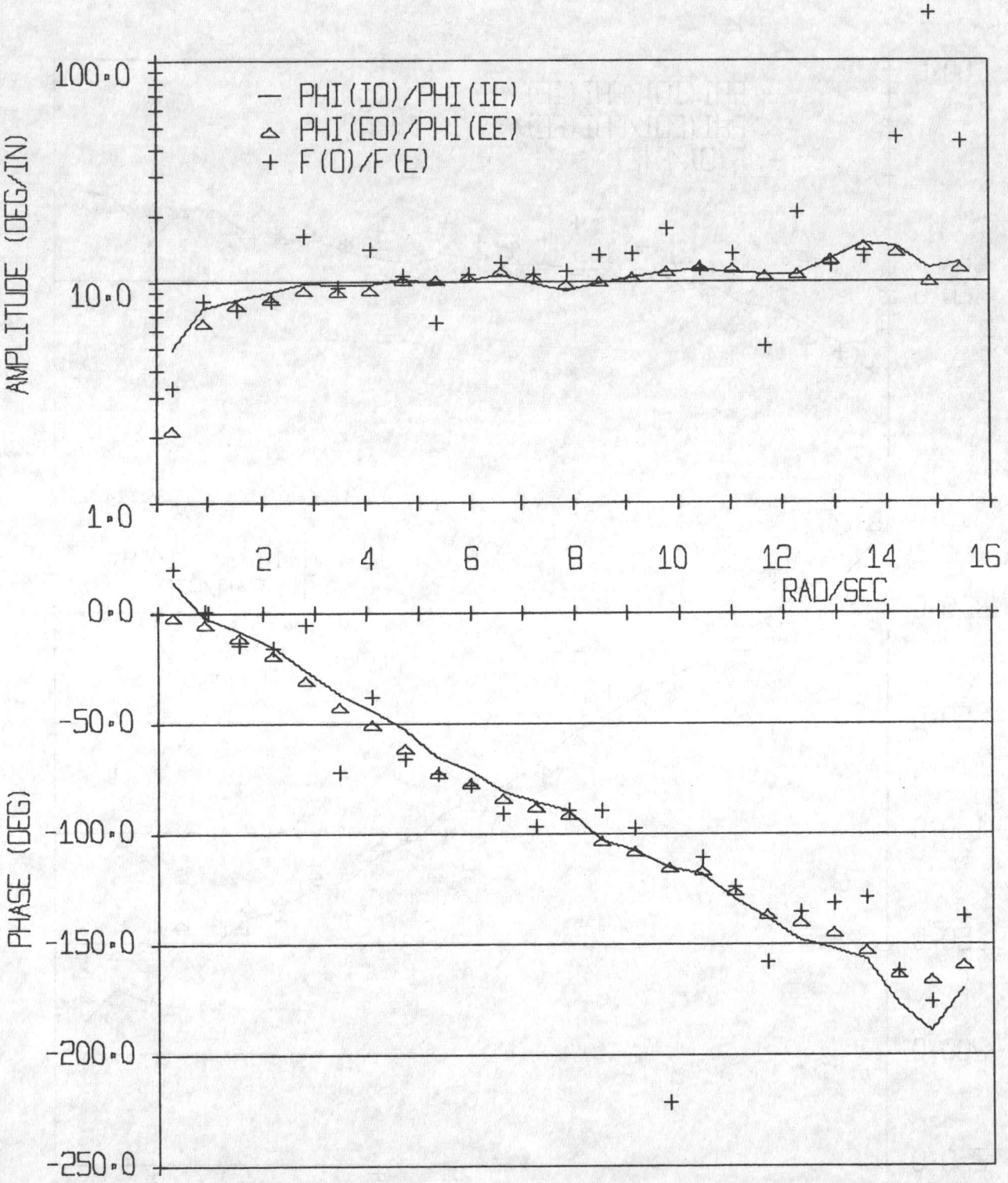


Figure 33 Comparison, one run, typical subject, M 1/s task.

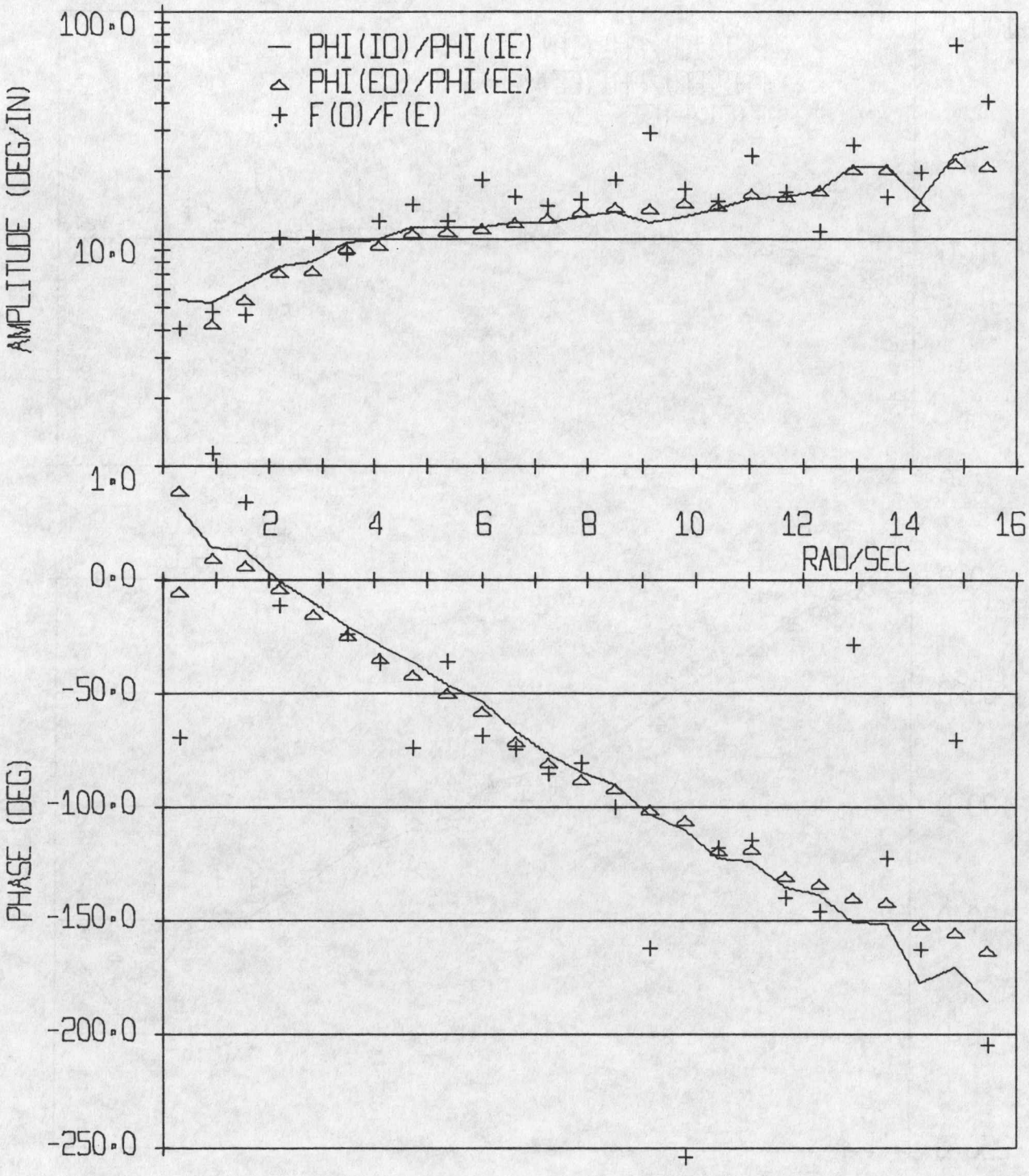


Figure 34 Comparison, one run, typical subject, H 1/s task.

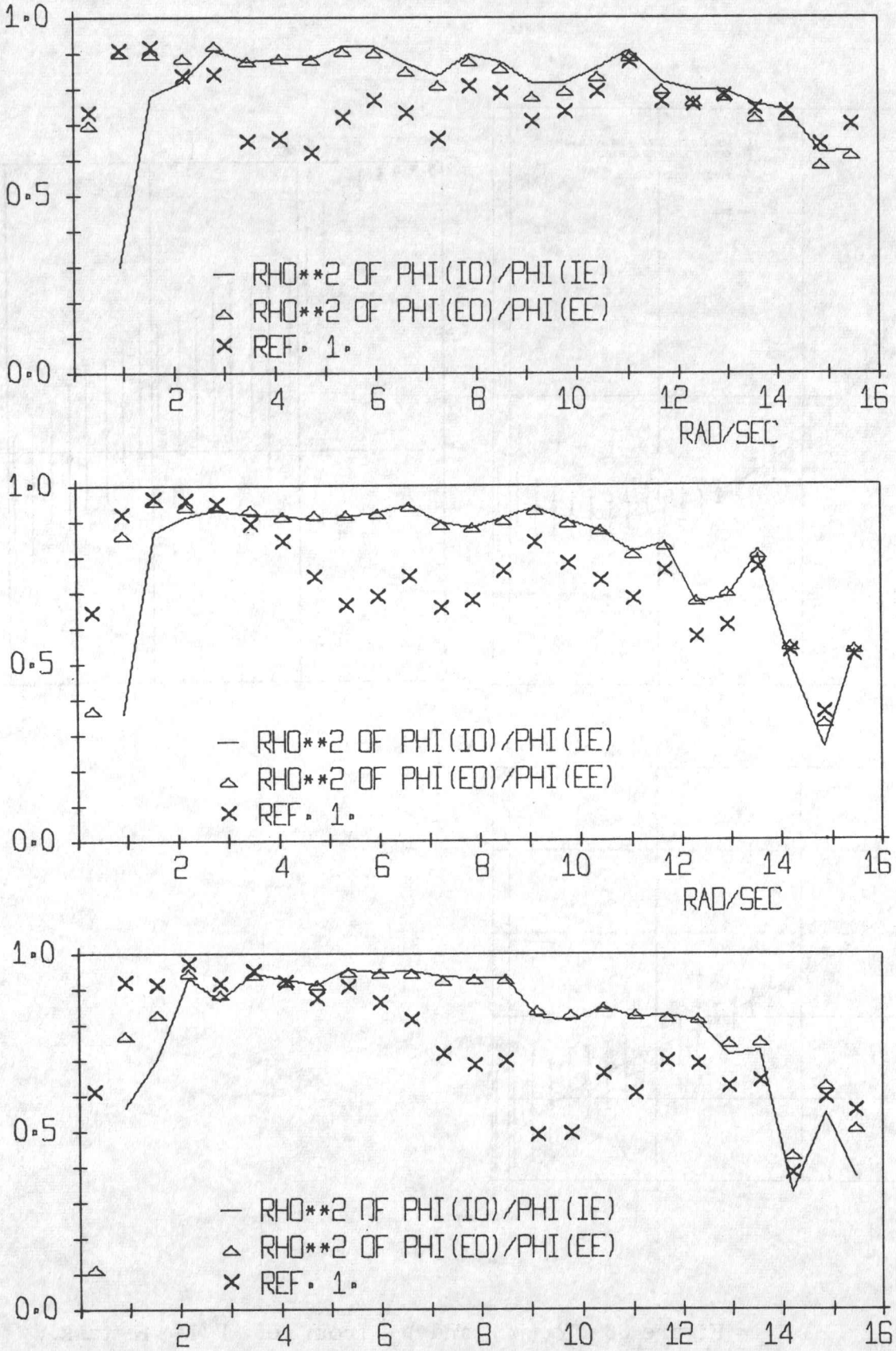


Figure 35 Comparison, one run, typical subject, L 1/s, M 1/s, and H 1/s task.

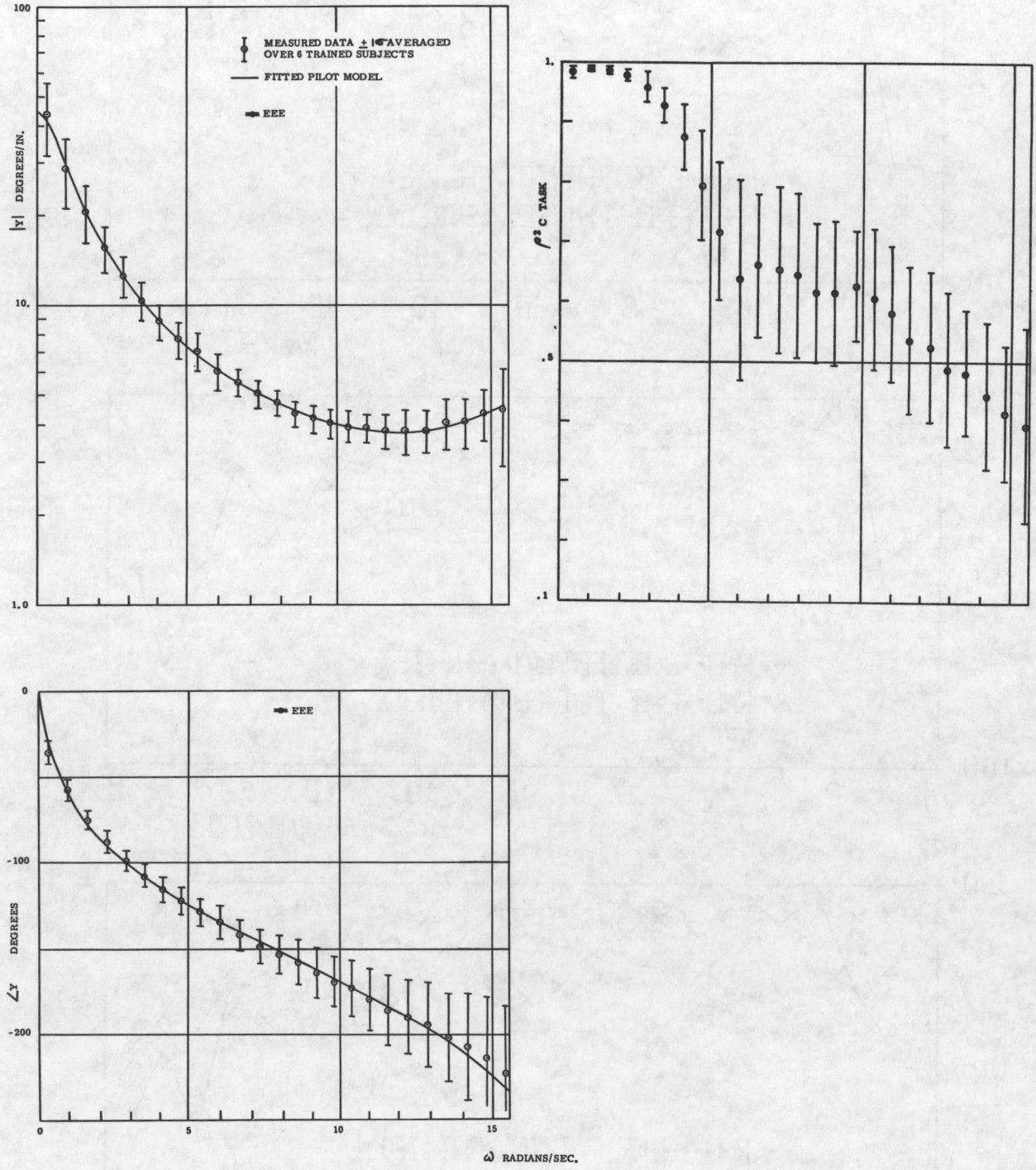


Figure 36 $Y_1(j\omega)$ and $\rho^2$ from ref. 1, M K task.

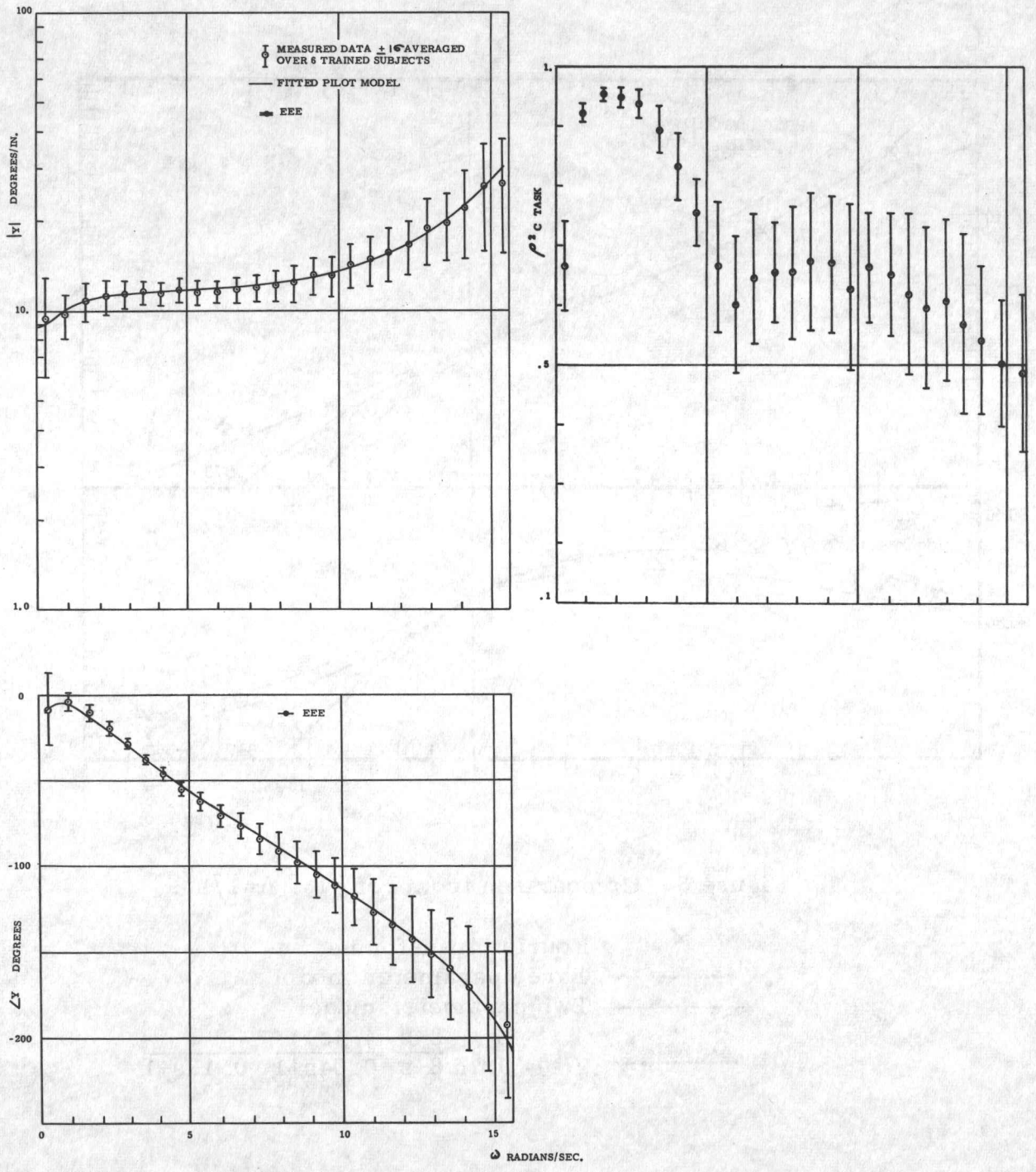


Figure 37 $Y_1(j\omega)$ and $\rho^2$ from ref. 1 . M 1/s task.

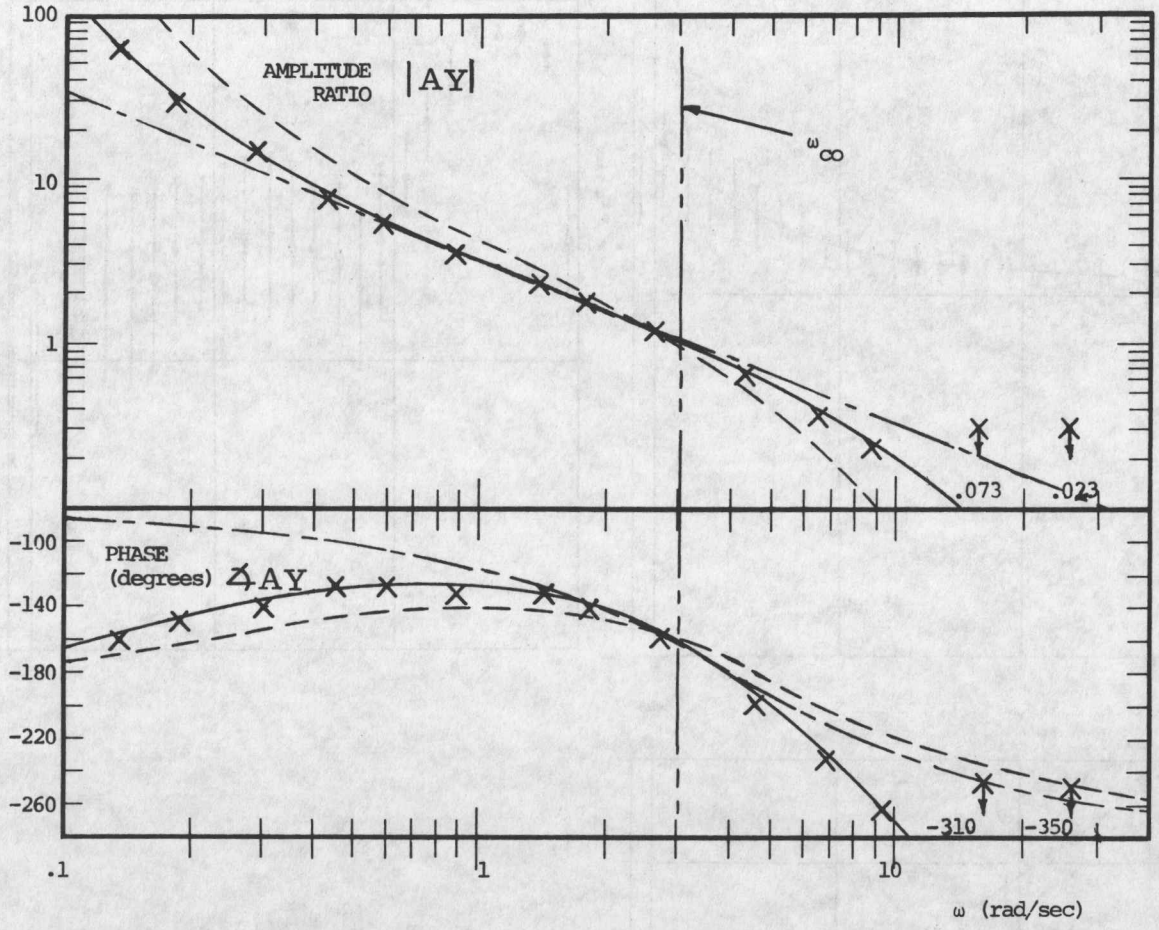


Figure 38 Comparison from ref. 16. $A=1/s^2$.

× Fourier transforms

— — — Three parameter model

– — – — Two parameter model

——— $Y(s)= 0.75 \frac{8-s}{8+s} \frac{4.4s+1}{0.04s+1} \frac{1}{0.12s+1}$

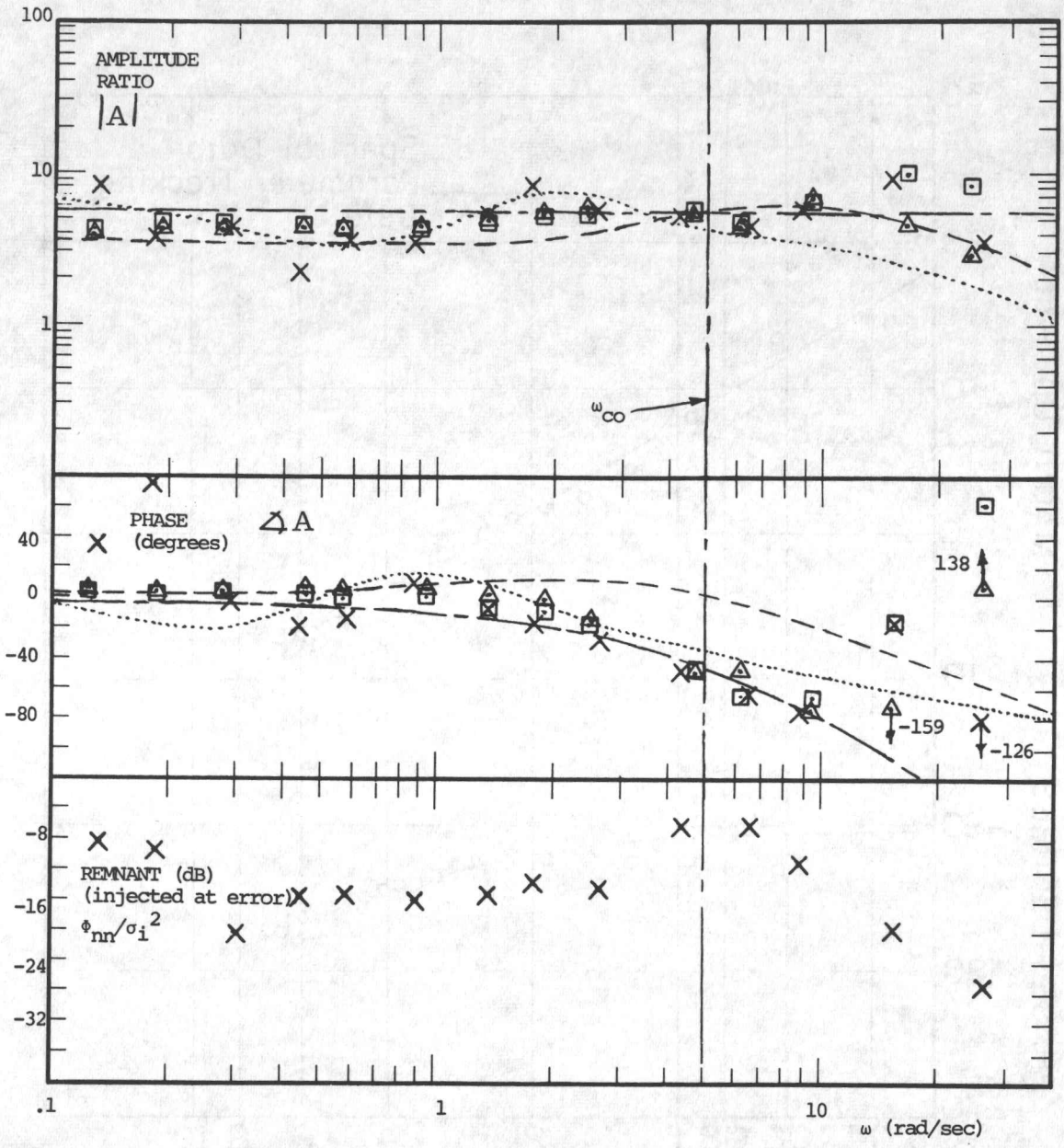


Figure 39 Comparison from ref. 16. A=1/s.

Fourier transforms
Three parameter model
Two parameter model
Orthogonal filters
Filtering and system realization
Cross Correlation

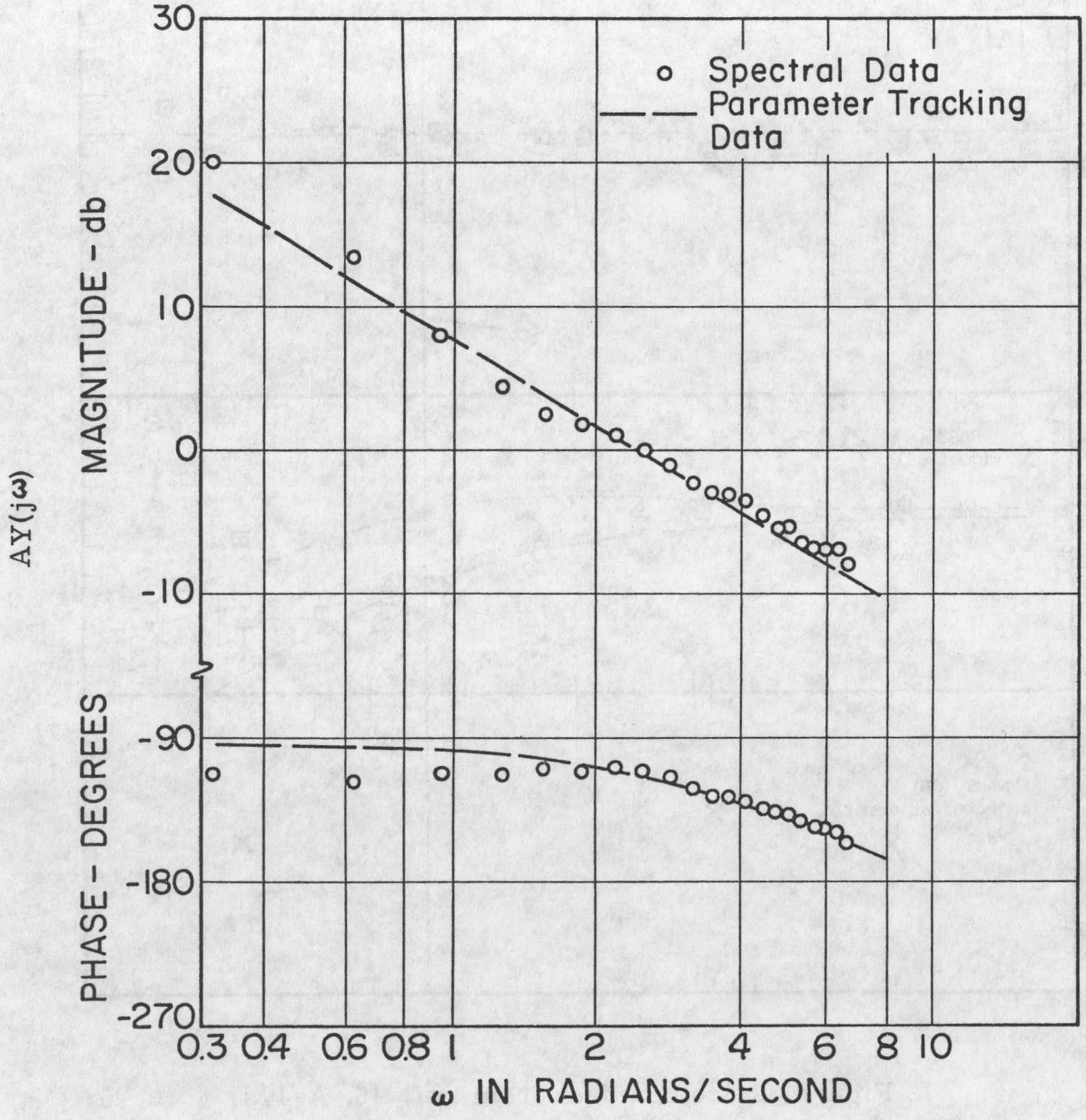


Figure 40 Comparison of Spectral and Parameter Tracking. M, 1/s Task.

UTIAS TECHNICAL NOTE NO. 167

## Institute for Aerospace Studies, University of Toronto

A COMPARISON OF PILOT DESCRIBING FUNCTION MEASUREMENT TECHNIQUES

Frostell, C. E. 14 pages 40 figures

1. Human Pilot Dynamics 2. Describing Function Measurements
3. Human Engineering
I. Frostell, C. E. II. UTIAS Technical Note No. 167

This work is aimed as assessing the techniques used to calculate human pilot describing functions. The study considers data analysis methods based on,

(a) cross power spectral density of pilot input, output and error;

(b) cross power spectral density of pilot output and error;

(c) Fourier transform of pilot output and error.

Taped records of human pilot performance from previous investigations in a compensatory control task with random input signals of continuous power spectra were on hand and provided a pilot data base. The same data were used to exercise each method, permitting direct comparison of the results. Data are presented as amplitude and phase plots of measured describing functions using an average of a reasonably large amount of data as well as single experimental runs. A comparison of the linear model fit parameter defined in two ways gave significant results.

Available copies of this report are limited. Return this card to UTIAS, if you require a copy.

UTIAS TECHNICAL NOTE NO. 167

Institute for Aerospace Studies, University of Toronto

A COMPARISON OF PILOT DESCRIBING FUNCTION MEASUREMENT TECHNIQUES

Frostell, C. E. 14 pages 40 figures

1. Human Pilot Dynamics 2. Describing Function Measurements
3. Human Engineering
I. Frostell, C. E. II. UTIAS Technical Note No. 167

This work is aimed as assessing the techniques used to calculate human pilot describing functions. The study considers data analysis methods based on,

(a) cross power spectral density of pilot input, output and error;

(b) cross power spectral density of pilot output and error;

(c) Fourier transform of pilot output and error.

Taped records of human pilot performance from previous investigations in a compensatory control task with random input signals of continuous power spectra were on hand and provided a pilot data base. The same data were used to exercise each method, permitting direct comparison of the results. Data are presented as amplitude and phase plots of measured describing functions using an average of a reasonably large amount of data as well as single experimental runs. A comparison of the linear model fit parameter defined in two ways gave significant results.

Available copies of this report are limited. Return this card to UTIAS, if you require a copy.

UTIAS TECHNICAL NOTE NO. 167

Institute for Aerospace Studies, University of Toronto

A COMPARISCN OF PILOT DESCRIBING FUNCTION MEASUREMENT TECHNIQUES

Frostell, C. E. 14 pages 40 figures

1. Human Pilot Dynamics 2. Describing Function Measurements
3. Human Engineering
I. Frostell, C. E. II. UTIAS Technical Note No. 167

This work is aimed as assessing the techniques used to calculate human pilot describing functions. The study considers data analysis methods based on,

(a) cross power spectral density of pilot input, output and error;

(b) cross power spectral density of pilot output and error;

(c) Fourier transform of pilot output and error.

Taped records of human pilot performance from previous investigations in a compensatory control task with random input signals of continuous power spectra were on hand and provided a pilot data base. The same data were used to exercise each method, permitting direct comparison of the results. Data are presented as amplitude and phase plots of measured describing functions using an average of a reasonably large amount of data as well as single experimental runs. A comparison of the linear model fit parameter defined in two ways gave significant results.

Available copies of this report are limited. Return this card to UTIAS, if you require a copy.

UTIAS TECHNICAL NOTE NO. 167

Institute for Aerospace Studies, University of Toronto

A COMPARISON OF PILOT DESCRIBING FUNCTION MEASUREMENT TECHNIQUES

Frostell, C. E. 14 pages 40 figures

1. Human Pilot Dynamics 2. Describing Function Measurements
3. Human Engineering
I. Frostell, C. E. II. UTIAS Technical Note No. 167

This work is aimed as assessing the techniques used to calculate human pilot describing functions. The study considers data analysis methods based on,

(a) cross power spectral density of pilot input, output and error;

(b) cross power spectral density of pilot output and error;

(c) Fourier transform of pilot output and error.

Taped records of human pilot performance from previous investigations in a compensatory control task with random input signals of continuous power spectra were on hand and provided a pilot data base. The same data were used to exercise each method, permitting direct comparison of the results. Data are presented as amplitude and phase plots of measured describing functions using an average of a reasonably large amount of data as well as single experimental runs. A comparison of the linear model fit parameter defined in two ways gave significant results.

Available copies of this report are limited. Return this card to UTIAS, if you require a copy.